Title

Transmembrane Helix Straightening and Buckling Underlies Activation of Mechanosensitive and Thermosensitive K2P Channels

Journal

Neuron, 84(6)

ISSN

0896-6273

Authors

Lolicato, Marco
Riegelhaupt, Paul M
Arrigoni, Cristina
et al.

Publication Date

2014-12-01

DOI

10.1016/j.neuron.2014.11.017

Peer reviewed

CellPress

Neuron
Article

Transmembrane Helix Straightening and Buckling Underlies Activation of Mechanosensitive and Thermosensitive K_{2P} Channels

Marco Lolicato,[1] Paul M. Riegelhaupt,[1,2] Cristina Arrigoni,[1] Kimberly A. Clark,[1] and Daniel L. Minor, Jr.[1,3,4,5,*]
[1]Cardiovascular Research Institute
[2]Department of Anesthesia and Perioperative Care
[3]Departments of Biochemistry and Biophysics, and Cellular and Molecular Pharmacology
[4]California Institute for Quantitative Biomedical Research
University of California, San Francisco, San Francisco, California 93858-2330, USA
[5]Physical Biosciences Division, Lawrence Berkeley National Laboratory, Berkeley, CA 94720, USA
*Correspondence: daniel.minor@ucsf.edu
http://dx.doi.org/10.1016/j.neuron.2014.11.017

SUMMARY

Mechanical and thermal activation of ion channels is central to touch, thermosensation, and pain. The TRAAK/TREK K_{2P} potassium channel subfamily produces background currents that alter neuronal excitability in response to pressure, temperature, signaling lipids, and anesthetics. How such diverse stimuli control channel function is unclear. Here we report structures of K_{2P}4.1 (TRAAK) bearing C-type gate-activating mutations that reveal a tilting and straightening of the M4 inner transmembrane helix and a buckling of the M2 transmembrane helix. These conformational changes move M4 in a direction opposite to that in classical potassium channel activation mechanisms and open a passage lateral to the pore that faces the lipid bilayer inner leaflet. Together, our findings uncover a unique aspect of K_{2P} modulation, indicate a means for how the K_{2P} C-terminal cytoplasmic domain affects the C-type gate which lies ~40Å away, and suggest how lipids and bilayer inner leaflet deformations may gate the channel.

INTRODUCTION

Detection of mechanical (Anishkin et al., 2014; Kung, 2005; Nilius and Honoré, 2012) and thermal (Bandell et al., 2007; Jordt et al., 2003; Vriens et al., 2014) stimuli is fundamental to the survival of both single-cell (Haswell et al., 2011; Kung et al., 2010) and multicellular organisms (Julius, 2013; Tsunozaki and Bautista, 2009). The ability to link mechanical and thermal changes with transmembrane ionic fluxes provides a direct means to couple stimulus detection to a rapid host response. Molecular studies have identified a diverse set of ion channels in the nervous system that have the capacity to detect and respond to mechanical and thermal cues. Members of the K_{2P} potassium channel family (Honoré, 2007; Nilius and Honoré, 2012; Noël et al., 2011), transient receptor potential (TRP) family (Anishkin et al., 2014; Julius, 2013; Kung, 2005; Vay et al., 2012; Vriens et al., 2014), and newly discovered Piezo channels (Bagriantsev et al., 2014; Nilius and Honoré, 2012) are thought to possess intrinsic mechanisms through which they detect and respond to pressure changes, temperature changes, or both. Although structural data have begun to become available for these families (Brohawn et al., 2012, 2013; Cao et al., 2013; Kamajaya et al., 2014; Liao et al., 2013), the molecular mechanisms by which such channels can detect and sense changes in pressure and temperature remain incompletely understood.

K_{2P} potassium channels generate leak currents that are important modulators of neuronal activity (Enyedi and Czirják, 2010; Lesage and Barhanin, 2011). Unlike voltage-gated or inward rectifier channels, K_{2P}s conduct ions over the entire physiological voltage range. Nevertheless, the magnitude of the leak current can be tuned by diverse inputs including natural effectors such as pressure, temperature, pH, lipids, and phosphorylation as well as exogenous agents such as anesthetics (Mathie et al., 2010). The mechanosensitive and thermosensitive subclass of K_{2P}s (Noël et al., 2011) comprising K_{2P}4.1 (TRAAK) (Maingret et al., 1999a), K_{2P}2.1 (TREK-1) (Dedman et al., 2009; Fink et al., 1996; Patel et al., 1998), and K_{2P}10.1 (TREK-2) (Bang et al., 2000; Lesage et al., 2000b), have particularly important roles in pain and anesthetic responses (Alloui et al., 2006; Noël et al., 2009; Patel et al., 1999; Pereira et al., 2014). K_{2P}4.1 (TRAAK) and K_{2P}2.1 (TREK-1) are also positively modulated by lipids such as lysophospholipids, polyunsaturated fatty acids such as arachidonic acid (AA), and phosphatidylinositol 4,5-bisphosphate (PIP_2) (Bang et al., 2000; Chemin et al., 2005a, 2005b, 2007; Fink et al., 1998; Lopes et al., 2005; Maingret et al., 2000b). The capability of this K_{2P} subclass to respond to both pressure (Bagriantsev et al., 2011; Brohawn et al., 2014; Kim et al., 2001b; Maingret et al., 1999a, 1999b; Noël et al., 2009; Patel et al., 1998) and temperature (Bagriantsev et al., 2011; Kang et al., 2005; Maingret et al., 2000a; Noël et al., 2009) raises the possibility that these two physical modalities feed into a common mechanism that controls channel function and is supported by recent studies (Bagriantsev et al., 2011, 2012).

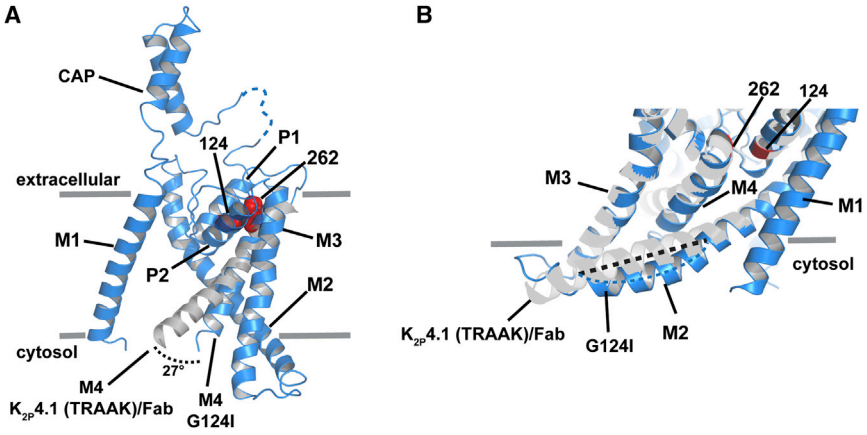

Figure 1. Structure of G124I K_{2P}4.1 (TRAAK)-Activating Mutant

(A and B) Superposition of chain A of G124I (marine) and K_{2P}4.1 (TRAAK) (gray) from the K_{2P}4.1 (TRAAK)/Fab complex (Brohawn et al., 2013) highlighting the conformational changes in the (A) M4 transmembrane helix and (B) M2 transmembrane helix. Dashed lines indicate differences in M2 for G124I (marine) and K_{2P}4.1 (TRAAK) (black). Key channel elements are indicated. Positions of residues 124 and 262 are indicated in red and are shown in space filling for the G124I structure in (A).

Functional investigation indicates that, unlike other classes of potassium channels, K_{2P}s use a "C-type" gate, comprising the selectivity filter, as the principal site of gating, rather than an intracellular obstruction (Bagriantsev et al., 2011, 2012; Cohen et al., 2008; Piechotta et al., 2011; Rapedius et al., 2012). This view is corroborated by recent K_{2P} crystal structures showing a basic architecture in which there is an unhindered path for ions from the cytoplasm to the selectivity filter (Brohawn et al., 2012, 2013; Miller and Long, 2012). Although crystallographic studies of K_{2P}4.1 (TRAAK) (Brohawn et al., 2012, 2013) and K_{2P}1.1 (TWIK-1) (Miller and Long, 2012) have revealed the overall architecture of the K_{2P} family, the functional states represented by these crystal structures have been unclear.

In the mechanosensitive and thermosensitive K_{2P} subfamily, a variety of studies indicate that the cytoplasmic C-terminal tail is an important element in controlling gating by pressure, temperature, intracellular pH, and phosphorylation (Bagriantsev et al., 2012; Chemin et al., 2005b; Honoré et al., 2002; Kim et al., 2001a, 2001b; Mathie et al., 2010). Mechanistic studies suggest that changes in the intracellular C-terminal tail are directly transmitted to the C-type gate via the pore-lining M4 helix (Bagriantsev et al., 2011, 2012). Here we find substantial alteration in the position of the M4 helix in structures bearing gain-of-function mutations in residues that support the selectivity filter and that activate the C-type gate of a variety of K_{2P}s. This conformational change is centered on a conserved glycine and repositions the M4 C-terminal end by ~27°. This large change in M4 position is associated with a buckling in the M2 transmembrane helix, disruption of interhelical packing between M2 and M3 transmembrane helices, and opens a wide pathway to the inner leaflet of the bilayer. Together, these structural transformations suggest how changes in the C-terminal tail can be transmitted to the pore and how bilayer deformations, lipids, and other hydrophobic modifiers of channel activity, such as anesthetics, may influence channel activity.

RESULTS

Structure and Function of K_{2P}4.1 (TRAAK) Mutants

We determined the crystal structures of two mutants of the human mechanosensitive, thermosensitive, and lipid-modulated K_{2P} channel, K_{2P}4.1 (TRAAK), G124I and W262S at 3.3Å and 3.4Å resolution, respectively (Figures 1 and S1 available online; Table 1). These mutations reside on the P1 pore helix that contacts the top of M4 (G124I) or on the complementary side of M4 facing P1 (W262S) (Figures 1, S1B, and S1C). Previous studies have demonstrated that analogous mutations activate the C-type gate of K_{2P}2.1 (TREK-1) (Bagriantsev et al., 2011, 2012) and alter the gating of a number of other K_{2P}s (Bagriantsev et al., 2011, 2012). Both mutants crystallized in the $P2_12_12_1$ space group having one channel dimer per asymmetric unit, comparable to the wild-type K_{2P}4.1 (TRAAK) crystals (Brohawn et al., 2012). The overall structures of G124I and W262S resemble the previously reported K_{2P}4.1 (TRAAK) structures (Brohawn et al., 2012, 2013) (Table S1). However, unlike a structure from a similar crystal habit (Brohawn et al., 2012), the M1 transmembrane helix is domain swapped in both mutants in a manner matching the domain swap seen in the K_{2P}4.1 (TRAAK)/Fab complex (Brohawn et al., 2013). This result supports the idea that the domain-swapped architecture is an intrinsic property of K_{2P}4.1 (TRAAK), and is not a consequence of Fab binding.

Cognate mutations to K_{2P}4.1 (TRAAK) G124I and W262S activate the closely related mechanosensitive and thermosensitive channel K_{2P}2.1 (TREK-1) (Bagriantsev et al., 2011, 2012). Hence, we anticipated that these mutants should activate K_{2P}4.1 (TRAAK) and affect modulation by various types of gating commands. Nevertheless, because these K_{2P}4.1 (TRAAK) mutants had not been previously characterized, we used patch clamp electrophysiology to examine how they affected responses to three stimuli known to activate K_{2P}4.1 (TRAAK): the polyunsaturated fatty acid AA (Brohawn et al., 2012; Fink et al., 1998; Kim et al., 2001a; Lesage et al., 2000a), the mechanosensitive and thermosensitive K_{2P} small-molecule activator ML67-33 (Bagriantsev et al., 2013), and membrane stretch (Brohawn et al., 2014; Lesage et al., 2000a; Maingret et al., 1999a). As expected, we found that both G124I and W262S blunted the K_{2P}4.1 (TRAAK) responses in a manner similar to the effects of the analogous changes on K_{2P}2.1 (TREK-1) (Bagriantsev et al., 2011, 2012) and in a manner consistent with channel activation (Figure 2). W262S reduced the ability of ML67-33 and pressure to activate the

Table 1. Crystallographic Data Collection and Refinement Statistics

Data Collection	K_{2P}4.1 (TRAAK) G124I	K_{2P}4.1 (TRAAK) W262S
Space group	$P2_12_12_1$	$P2_12_12_1$
Cell dimensions a/b/c (Å)	87.5/118.7/128.7	88.1/125.1/130.0
α/β/γ (°)	90.0/90.0/90.0	90.0/90.0/90.0
Resolution (Å)	49.11–3.30 (3.56–3.30)	48.31–3.4 (3.67–3.4)
R_{sym} (%)	11.9 (> 100%)	11.7 (> 100%)
I/σ I	6.6 (0.4)	4.0 (0.2)
Correlation coefficient	0.997 (0.133)	0.994 (0.125)
Completeness (%)	100.0 (99.0)	100.0 (100.0)
Redundancy	41.0 (34.3)	13.4 (12.9)
Unique reflections	20,804	20,452
Wilson B factor	134.84	130.39
Refinement		
R_{work}/R_{free} (%)	29.1/32.3	29.7/32.8
No. of chains in AU	2	2
No. of protein atoms	3,887	3,908
No. of ligand atoms	6	6
No. of water atoms	0	0
RMSD bond lengths (Å)	0.003	0.003
RMSD angles (°)	0.677	0.801
Ramachandran best/ disallowed regions (%)	92.0/0.4	92.6/0.2

channel, but had a modest effect on AA stimulation (Figures 2B, 2D, and 2E). By contrast, G124I effectively rendered the channel insensitive to further activation by any of the stimuli (Figures 2C–2E). This rank order matches that seen for the analogous K_{2P}2.1 (TREK-1) mutants (Bagriantsev et al., 2012), and given the similarities between K_{2P}4.1 (TRAAK) and K_{2P}2.1 (TREK-1), suggests that the G124I and W262S structures represent conformations adopted by an activated K_{2P} channel.

Pore-Lining M4 Helix of Activating Mutants Bends and Twists around a Conserved Glycine

The conformations of the two polypeptide chains comprising the G124I and W262S channels are nonidentical (Figures S2A and S2B). The largest structural asymmetry occurs in the lower half of the channel and is most evident in the conformations of intracellular portions of M2, M3, and M4 helices. Similar conformational heterogeneity was also seen in the structures of K_{2P}4.1 (TRAAK) (Brohawn et al., 2012) and K_{2P}4.1 (TRAAK)/Fab complex (Brohawn et al., 2013). It is notable that in all of these cases, one chain of the dimer, chain B, makes substantial crystal lattice contacts through interactions of the intracellular parts of M2, M3, and M4 with either the extracellular CAP domain or Fab from another channel complex in the crystal lattice (Figure S3). By contrast, chain A is unhindered, and thus, we focused our initial analysis on comparisons of this chain in each of the structures.

The changes in the vicinity of the mutations in the G124I and W262S structures appear modest. In both, the N-terminal end of M4 is closer to the P1 helix when compared with the K_{2P}4.1 (TRAAK)/Fab complex (Figure S1B). Additionally, in both chains of the G124I structure, the Trp262 side chain undergoes a rotamer switch that matches that seen in chain A of the K_{2P}4.1 (TRAAK)/Fab complex (Brohawn et al., 2013, 2014) (Figures S1B and S1C). This local change avoids a clash with the increased size of the akyl side chain at G124I and is consistent with the idea of cross-talk between the P1 pore helix and M4 transmembrane helix at these two positions (Bagriantsev et al., 2012).

In contrast to the modest structural changes near the mutation sites, we observe substantial conformational changes in elements of the channel distant from the G124I and W262S mutations. These alterations are most pronounced in the G124I mutant (Figures 1A, 1B, and S2). Prior structure determinations of K_{2P}4.1 (TRAAK) revealed differences in the position of the M4 pore-lining helix of the unrestrained subunit (Brohawn et al., 2012, 2013). This channel element adopts an elevated position that closes one of the lateral openings to the bilayer in the K_{2P}4.1 (TRAAK)/Fab complex structure (Brohawn et al., 2013). We take this conformation as the reference for analyzing G124I and W262S.

In both K_{2P}4.1 (TRAAK) G124I and W262S, the pore-lining M4 helix is much straighter than either of the conformations observed in the wild-type K_{2P}4.1 (TRAAK) structures (Figures 1A, 3A, and 3B) and is tilted by ~27° and ~23°, respectively, relative to K_{2P}4.1 (TRAAK)/Fab complex M4. This change leads to a movement of ~8.3Å of Asn281, which is the last common residue visible among the G124I, W262S, and K_{2P}4.1 (TRAAK)/Fab complex structures. These differences are much greater than the ~11° difference between the two wild-type K_{2P}4.1 (TRAAK) structures (Figure 3B). M4 tilting is accompanied by a loss of helical structure over its last two turns (Figures 3A, 3B, and S4A). Additionally, the G124I helix has a slight counterclockwise twist when viewed from the N-terminal end. The M4 tilt in G124I and W262S is centered on Gly268 (Figure 3A). This residue is strictly conserved across all K_{2P}s (Figure S4A) and corresponds to a conserved glycine in the pore-lining helix that is central to the gating of diverse classes of potassium channels (Bavro et al., 2012; Cuello et al., 2010a; Jiang et al., 2002; Magidovich and Yifrach, 2004; Uysal et al., 2009). Notably, this position also matches the glycine at the center of crystallographically observed bending motions of multiple conformational states of the pore-lining helices of KcsA (Cuello et al., 2010a, 2010b; Uysal et al., 2009) and KirBac3.1 (Bavro et al., 2012) that are related to activation gating.

Superposition of the N-terminal portions of all K_{2P}4.1 (TRAAK) M4s reveals a family of conformations C terminal to Gly268 in which the unhindered "A" chains from the K_{2P}4.1 (TRAAK)/Fab complex and G124I structures represent the extremes (Figure 3C). M4 helices from all of the "B" chains populate the center of this distribution, are quite similar, and largely follow the path of the W262S mutant (Figure 3C). The observation of this family of M4 conformations demonstrates that this helix can make graded changes between the bent K_{2P}4.1 (TRAAK)/Fab complex chain A conformation and the G124I straight conformation. Notably, the degree of bending is similar to that described for a series of KcsA

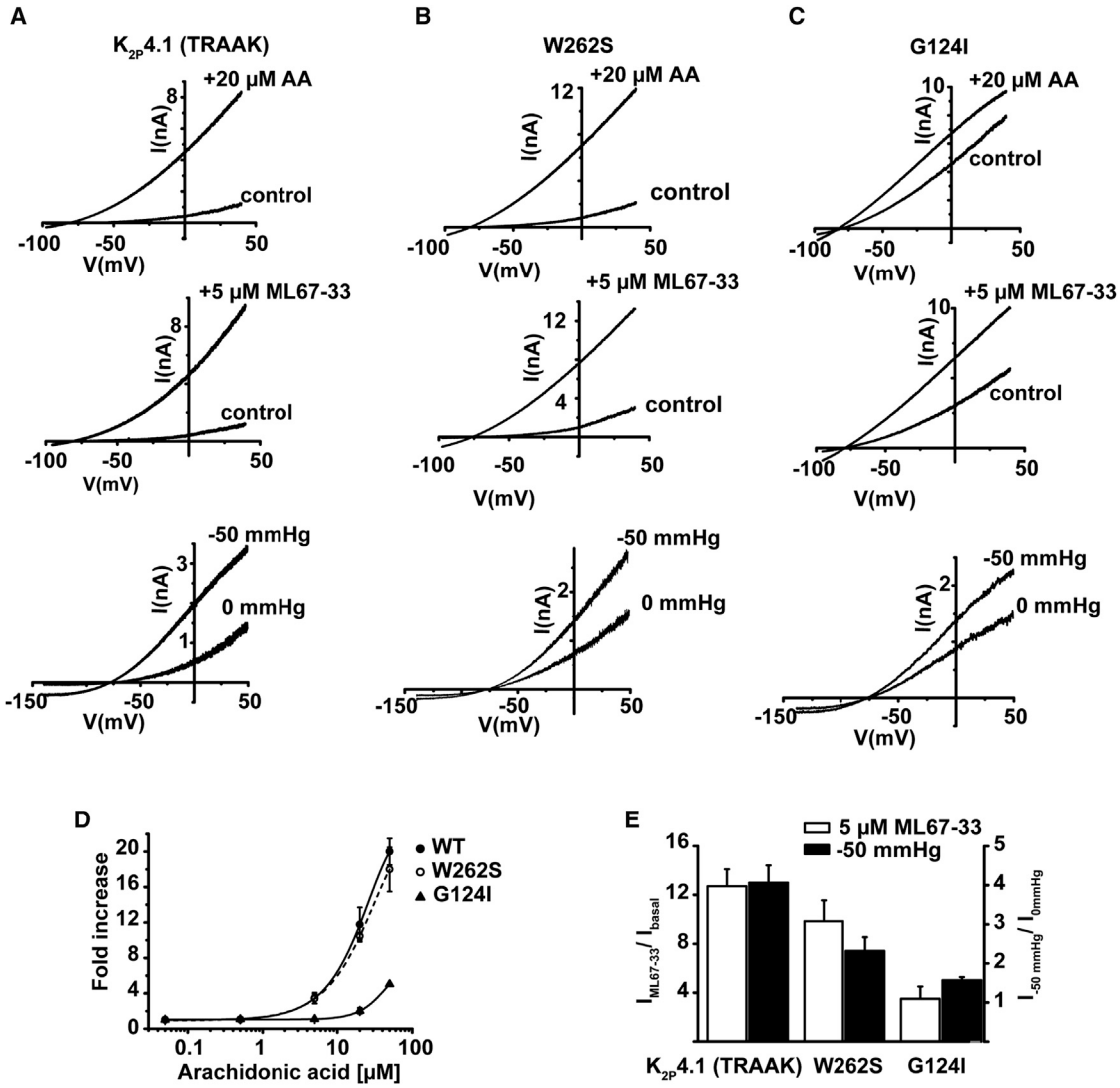

Figure 2. Gain-of-Function Effects of W262S and G124I

(A–C) Exemplar whole-cell patch-clamp responses of (A) K_{2P}4.1 (TRAAK), (B) W262S, and (C) G124I expressed in HEK293 cells to stimulation by arachidonic acid (AA), ML67-33 (Bagriantsev et al., 2013), and membrane stretch.

(D) AA dose response for the indicated channels measured at 0 mV. Potentiation by 20 μM AA was as follows: K_{2P}4.1 (TRAAK) 11.7 ± 1.9; G124I 2.0 ± 0.3; W262S 10.4 ± 0.4.

(E) Current potentiation measured at 0 mV for K_{2P}4.1 (TRAAK), G124I, and W262S in response to 5 μM ML67-33 (K_{2P}4.1 (TRAAK) 12.7 ± 1.4; G124I 3.5 ± 1.0; W262S 9.8 ± 1.7) and −50 mm Hg pressure (K_{2P}4.1 (TRAAK) 4.1 ± 0.4; G124I 1.57 ± 0.07; W262S 2.3 ± 0.3). For all experiments basal currents were ≥ 500 pA and n ≥ 4. Data are mean ± SEM.

structures (Cuello et al., 2010b). However, unlike in KcsA (Cuello et al., 2010a, 2010b; Uysal et al., 2009) and KirBac3.1 (Bavro et al., 2012) where closed channels have a straight pore-lining helix that forms an intracellular gate and bend into the activated conformation, activated K_{2P}4.1 (TRAAK) mutants have a straight pore-lining helix.

M4 Movement Correlates with the Extent of M2 Buckling at a Conserved GXG

The K_{2P}4.1 (TRAAK) M2 transmembrane helix is unusual. It is longer than the other transmembrane helices and has a kink at Pro155 that causes it to run somewhat parallel to the plane of the membrane below the selectivity filter (Brohawn et al., 2012). In the G124I structure, M4 movement is accompanied by a displacement and flexing of M2 at the point where it contacts M4 in a manner that resembles a buckling motion (Figures 1B, 4A, and 4B). This disruption of the helix begins at K_{2P}4.1 (TRAAK) residues 163–165, a "GXG" sequence that is conserved within the subfamily of mechanosensitive- and temperature-sensitive K_{2P}s (K_{2P}4.1 (TRAAK), K_{2P}2.1 (TREK-1), and K_{2P}10.1 (TREK-2)) (Figure S4B), and propagates over four helical turns into the loop beginning at Trp186 that joins the M2 and M3

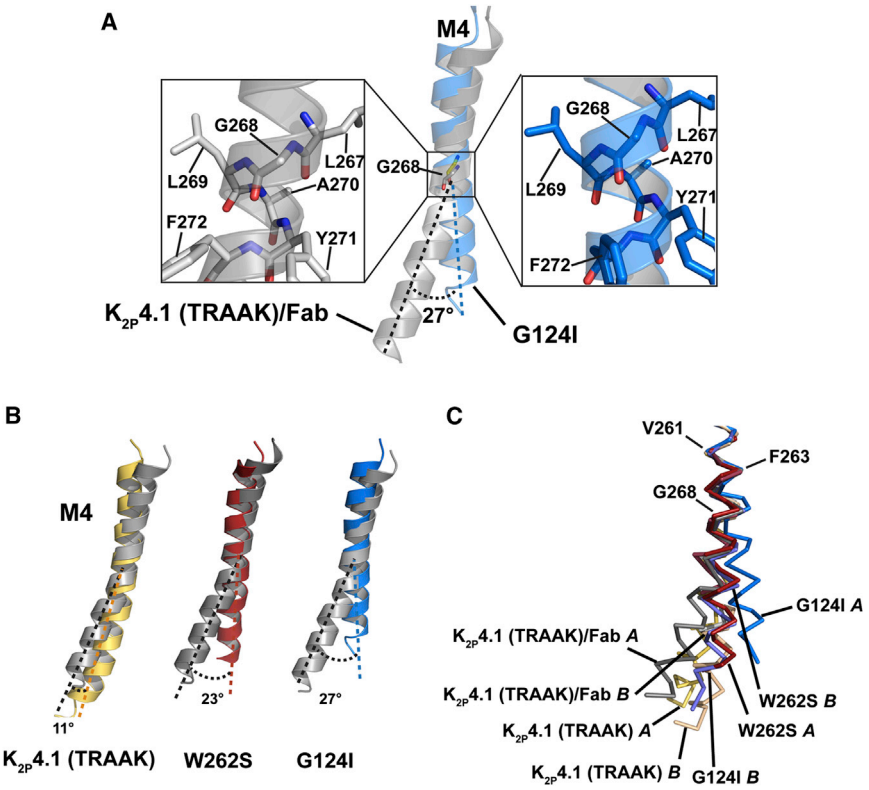

Figure 3. Structural Changes in M4

(A) Superposition of M4 helix from G124I (marine) and K_{2P}4.1 (TRAAK) (gray) from the K_{2P}4.1 (TRAAK)/Fab complex (Brohawn et al., 2013) within the context of the full channel. Insets show region around Gly268.

(B) Comparison of the M4 helix conformations of K_{2P}4.1 (TRAAK) (Brohawn et al., 2012) (yellow), W262S (firebrick), and G124I (marine) with K_{2P}4.1 (TRAAK) from the Fab complex (Brohawn et al., 2013) (gray). Extent of changes in C-terminal end of M4 are indicated.

(C) Superposition of M4 helices from the indicated structures and chains using residues 256–263 in the helix N-terminal end.

helices (Figures 4A and 4B). Besides being strictly conserved in the mechanosensitive and thermosensitive K_{2P} subfamily, a variant of the GXG sequence in which the first residue is replaced by a small amino acid is found in all TASK channels (K_{2P}3.1 (TASK-1), K_{2P}9.1 (TASK-3), K_{2P}5.1 (TASK-2), and K_{2P}7.1 (TASK-5)) (Figure S4B).

M2 buckling leads to a displacement of the helix toward the cytoplasmic face of the channel (Figure 4B). In the region of largest perturbation, from Ser170 to Ile176, the M2 Cα positions move by a distance that is greater than a helix diameter (~5.2–5.6Å) and undergo an ~10° twist toward the cytoplasmic face. Local buckling of the M2 helix also occurs in the W262S mutant, but to a more limited extent, similarly beginning at Gly163 and propagating to Ile179, rather than into the M2-M3 loop (Figure 4C). The K_{2P}4.1 (TRAAK) structure also has a similar, but smaller, distortion beginning at Gly163 and ending at Leu168. These large differences in M2 are mostly absent in chain B (Figure S5). Taken together, the structures show that the extent of M2 buckling matches with the extent of M4 helix straightening and suggest that these two conformational changes are coupled (Movie S1).

Quaternary Changes between Resting and Activated States Open a Side Door to the Membrane

The conformational changes in M4 and M2 have a number of striking consequences for the channel quaternary structure. Comparison of the M4 position between its two extreme conformations seen in the K_{2P}4.1 (TRAAK)/Fab complex and G124I shows that in the elevated conformation, M4 of one subunit contacts M2 of the other subunit along a hydrophobic interface formed between M2 residues Leu151, Val152, Pro155, Leu156, and Ile159 and M4 residues Phe272, Leu276, Ile279, and Leu283 (Figure 5A). This configuration likely resembles the resting position of the activation gate in the absence of stimuli. This interface is disrupted when M4 straightens to the G124I conformation (Figure 5B). Once straightened, M4 makes a new set of interactions with both M2 and M3 of its own subunit. The largest changes are for Phe272/M4, which interacts with the backbone of Cys206/M3, and Val275/M4, which interacts with Phe201/M3 and Leu202/M3 (Figures 5C and 5D). The consequence of these changes is that the so-called "side window" that has been proposed as an interaction site for hydrophobic modulators such as lipids (Brohawn et al., 2012) and that is present in the K_{2P}4.1 (TRAAK) structure (Brohawn et al., 2012), but closed in the K_{2P}4.1 (TRAAK)/Fab complex (Brohawn et al., 2013), transforms into a completely open "door." This door is framed by residues from M2 of one subunit and the base of pore helix 2 and residues from M4 of the neighboring subunit (Movies S2 and S3). This door is completely lined by hydrophobic residues (Figure 5B) and would seem to provide a natural place for the binding of lipids in the inner leaflet of the bilayer or for activating compounds. It is striking that this dramatic architectural change could allow easy lipid access without requiring a reorientation of the lipids from their natural poses in which the hydrophilic head is on the cytoplasmic side of the bilayer, and the hydrophobic tails are in the membrane core.

A second effect of M4 movement is that the M2 buckling disrupts the interface between M2 and M3 formed by residues Ser197, Phe201, Il204, Leu168, Leu172, and Ile176 in the K_{2P}4.1 (TRAAK)/Fab complex (Figures 5E and 5F). In this disruption, Leu172 translates toward the cytoplasmic side, occupies the position formerly held by Ile176, and makes hydrophobic interactions with Phe201. Ile176 moves out of the interface and makes no new protein-protein interactions. Finally, when viewed from the cytoplasmic side, the structural changes result in a

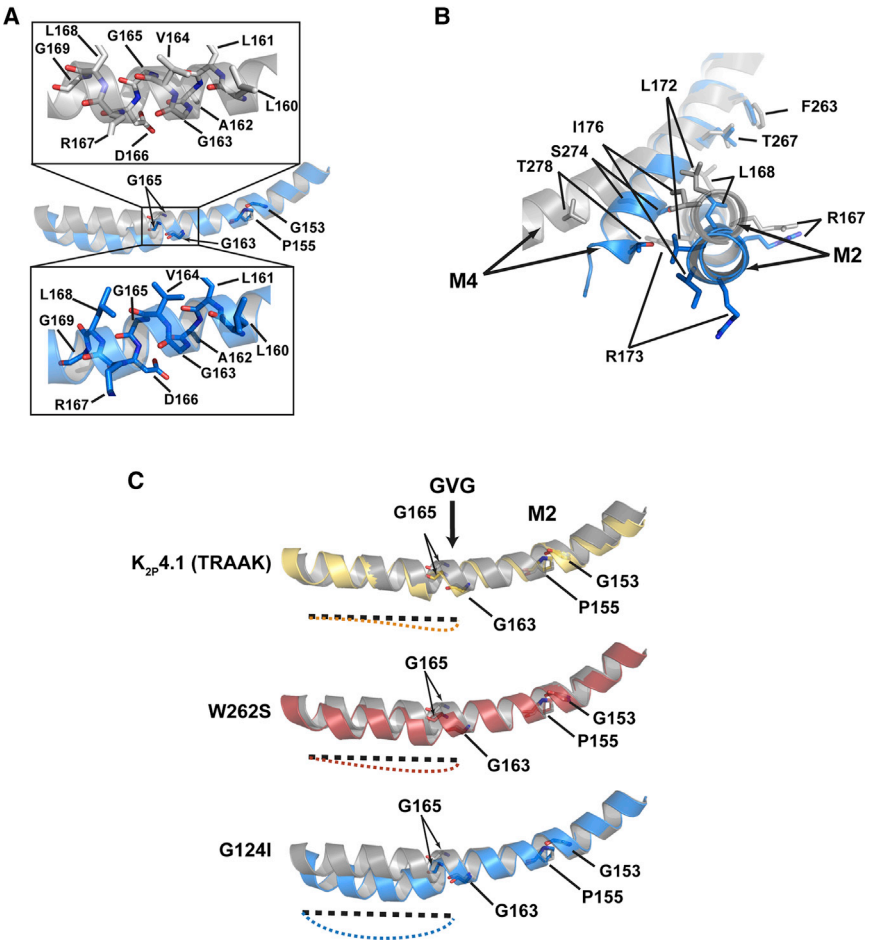

Figure 4. Structural Changes in M2

(A) Superposition of the M2 helix from G124I (marine) and K_{2P}4.1 (TRAAK) (gray) from the K_{2P}4.1 (TRAAK)/Fab complex (Brohawn et al., 2013). Insets show region around the GVG sequence.

(B) View showing the displacement and rotation of M2 in G124I (marine) toward the cytoplasmic side of the bilayer relative to K_{2P}4.1 (TRAAK) (gray). Residue pairs showing large changes are indicated by pairs of lines pointing to each position.

(C) Comparison of the M2 helix conformation of K_{2P}4.1 (TRAAK) (Brohawn et al., 2012) (yellow), W262S (firebrick), and G124I (marine) with with K_{2P}4.1 (TRAAK) from the Fab complex (Brohawn et al., 2013) (gray). Dashed lines highlight the regions of local helix buckling in each of the structures. Select residues are indicated.

substantial repositioning of the C-terminal end of M4. As this part of the protein is directly connected to the C-terminal tail, such movement offers a clear means for how changes in the status of the C-terminal tail can be propagated to the C-type gate via M4 as previously suggested from functional studies (Bagriantsev et al., 2012).

Currently, the only other structural information for the K_{2P} family comes from studies of K_{2P}1.1 (TWIK-1), a channel that is insensitive to mechano- or thermal activation and whose crystal structure is thought to represent an open state (Miller and Long, 2012). In this regard, it is especially striking that the M4 positions of the K_{2P}4.1 (TRAAK) G124I and W262S gain-of-function mutants superpose well with the K_{2P}1.1 (TWIK-1) M4 (Figures 6A and 6B). The K_{2P}1.1 (TWIK-1) structure showed an M4 helix leading to a loop that is followed by a short helix running parallel to the expected membrane inner leaflet, the C-helix. This transition starts at K_{2P}1.1 (TWIK-1) Leu270, a residue that is structurally equivalent to K_{2P}4.1 (TRAAK) Leu283, which is the last visible residue in the W262S mutant. Interestingly, W262S has an M4 position that is more similar to K_{2P}1.1 (TWIK-1) M4 than G124I. The K_{2P}1.1 (TWIK-1) M2 helix is shorter than that of K_{2P}4.1 (TRAAK), but follows the general direction of the buckled M2 of W262S and G124I, rather than the more gently curved path of the K_{2P}4.1 (TRAAK)/Fab M2 (Figure 6C). Consequently, its position relative to the cytoplasmic face of the channel is intermediate between the displaced position of the G124I M2 and that of K_{2P}4.1 (TRAAK)/Fab (Figure 6D). The conformational snapshots of K_{2P}4.1 (TRAAK) revealed by the two wild-type and two mutant structures, taken together with the similarities of the G124I and W262S structures with a likely open state channel represented by K_{2P}1.1 (TWIK-1), suggest that the series of K_{2P}4.1 (TRAAK) structures characterizes the conformations that link the channel resting state, embodied by the K_{2P}4.1 (TRAAK)/Fab complex, and the activated state, exemplified by G124I.

The Hydrophobic Face of the M2 Helix Is Important for Thermal Responses and Couples to the C-Type Gate

The most unexpected structural change in K_{2P}4.1 (TRAAK) G124I and W262S is the buckling of the M2 helix that occurs concomitantly with M4 straightening (Figure 4). Given these findings and the absence of prior functional studies aimed at the K_{2P} M2 helix, we set out to test the importance of key M2 features for channel function. Because coupling between various channel elements and the C-type gate is readily measured in the closely related mechanosensitive and thermosensitive channel K_{2P}2.1 (TREK-1) (Bagriantsev et al., 2011, 2012; Cohen et al., 2008), we used K_{2P}2.1 (TREK-1) to investigate the consequences of disruption of the M2/M3 interface and glycine of the GXG sequence that initiates the M2 buckling.

Alanine-scanning mutagenesis along the portion of the K_{2P}2.1 (TREK-1) M2 helix involved in the observed structural buckling of K_{2P}4.1 (TRAAK) revealed enhanced baseline channel activity from substitutions at positions comprising the M2/M3 interface, Leu181, Gly182, Phe185, and Ile189, but no effects from changes to residues residing on the opposite face of the M2 helix (Figures 7A and 7B). Because prior studies have established a

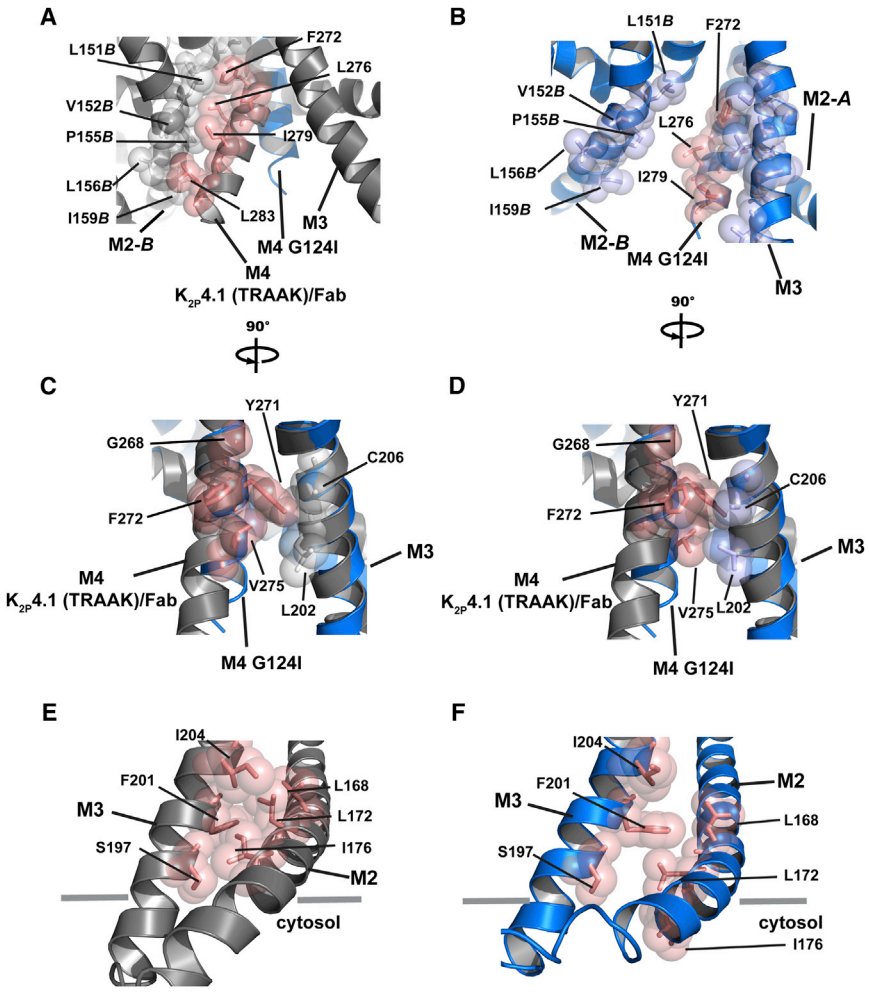

Figure 5. Quaternary Changes Associated with M4 and M2 Movements

(A and B) Intersubunit interactions made between M4 and M2 in the (A) K_{2P}4.1 (TRAAK)/Fab complex (Brohawn et al., 2013) that are broken in the (B) G124I M4 structure. Position of the G124I M4 helix is indicated in (A).

(C and D) Comparison of M4 residues in (C) the K_{2P}4.1 (TRAAK)/Fab complex (Brohawn et al., 2013) that gain interactions in (D) G124I. View is 90° to (A) and (B).

(E and F) Views of the M2/M3 interface in the (E) K_{2P}4.1 (TRAAK)/Fab complex (Brohawn et al., 2013) and (F) G124I. In all panels, key residues (red) are shown as clear space filling and sticks and are indicated.

clear correlation between increased baseline activity and C-type gate stabilization (Bagriantsev et al., 2011, 2012), these data suggest that disruption of the hydrophobic packing between M2 and M3 is important for channel activation. To test this idea directly, we examined the stability of the C-type gate to closure by extracellular acidosis (Bagriantsev et al., 2011, 2012; Clarke et al., 2008; Cohen et al., 2008; Lopes et al., 2000; Niemeyer et al., 2010) for two of the interface mutants that correspond to positions most affected by the rearrangement, K_{2P}2.1 (TREK-1) F185A and I189A, and the double mutant F185A/I189A. All of these changes stabilized the C-type gate to closure by acidic pH, with the largest change observed in the double mutant (Figure 7C) (pH_O IC_{50} = 7.51 ± 0.03, 7.27 ± 0.07, 7.15 ± 0.10, 7.00 ± 0.14 for wild-type, F185A, I189A, and F185A/I189A, respectively). Furthermore, examination of the temperature responses of these channels shows that they have blunted responses to temperature increases, with the strongest effect being found in the F185A/I189A (Figure 7D). Taken together, these data support the idea that disruption of the M2/M3 interface caused by M2 helix buckling is central to channel activation and is coupled to stabilization of the C-type gate.

Having established the link between the M2/M3 interface with C-type gate stabilization and altered thermal responses, we next investigated the importance of the most conserved element of the GXG motif, the second glycine corresponding to K_{2P}4.1 (TRAAK) Gly165. This residue appears to be a key point in allowing the helix to bulge (Figure 4A) and is conserved in the mechanosensitive and thermosensitive subfamily as well as in the TASK channels (Figure S4B). To investigate this position, we examined the consequences of enabling or inhibiting the ability of this residue to be distorted within the context of the M2 helix by substituting the Gly165 equivalent of K_{2P}2.1 (TREK-1), Gly178, with two amino acids, one that should facilitate kinking, proline (Cordes et al., 2002; Yohannan et al., 2004a, 2004b), and one that should inhibit helix kinking, alanine (Faham et al., 2004). Tests of the temperature responses revealed channels that behaved exactly as expected if the kink at the second GXG glycine is important for activation (Figures 7E and 7F). G178P channels were activated, whereas the currents of the G178A mutants were suppressed and showed a greatly diminished temperature response relative to wild-type. Taken together, these results are entirely consistent with the inferences derived from the K_{2P}4.1 (TRAAK) structures and support the idea that the bending and buckling of M2 is an essential part of activation of mechanoactivated and thermoactivated channels from the TREK/TRAAK subfamily.

DISCUSSION

Investigation of the molecular mechanisms by which pressure (Anishkin et al., 2014; Kung, 2005) and temperature (Chowdhury et al., 2014; Clapham and Miller, 2011) changes affect channel gating is one of intense current focus. Channels from the K_{2P} subfamily encompassing K_{2P}4.1 (TRAAK), K_{2P}2.1 (TREK-1), and K_{2P}10.1 (TREK-2) are notable for being activated by both temperature and mechanical cues (Dedman et al., 2009; Noël et al., 2011). Hence, mechanistic studies of this subclass should not only provide insights into how these particular channels

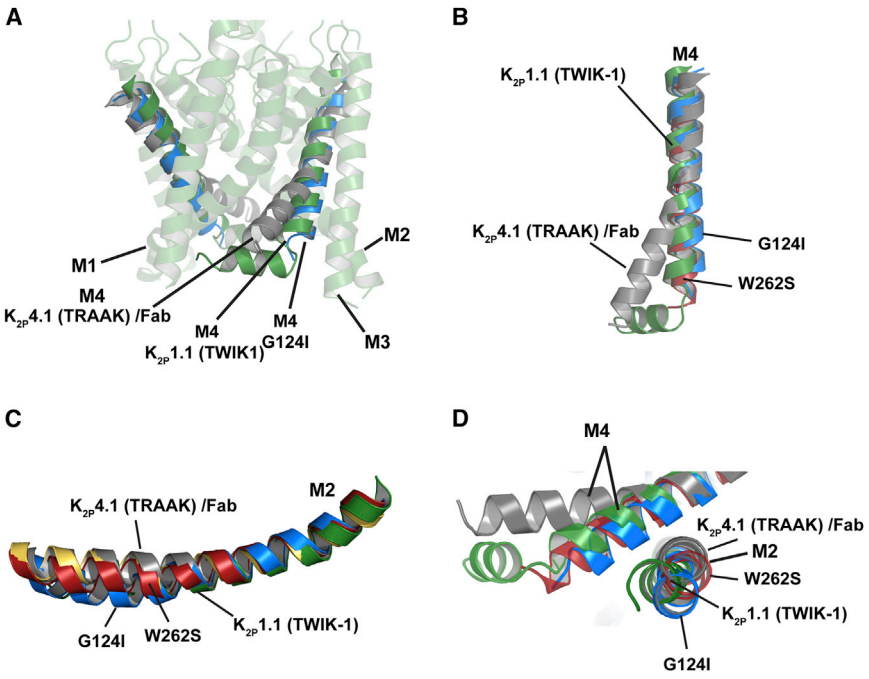

Figure 6. Structural Comparisons with K_{2P}1.1 (TWIK-1)

(A) Comparison of the K_{2P}4.1 (TRAAK)/Fab complex (Brohawn et al., 2013) (gray) and G124I (marine) M4 helices in the context of K_{2P}1.1 (TWIK-1) (Miller and Long, 2012) (green).

(B) Comparison of M4 helices from K_{2P}4.1 (TRAAK)/Fab complex (Brohawn et al., 2013) (gray), G124I (marine), W262S (firebrick), and of K_{2P}1.1 (TWIK-1) (Miller and Long, 2012) (green).

(C) Comparison of M2 helices from K_{2P}4.1 (TRAAK)/Fab complex (Brohawn et al., 2013) (gray), G124I (marine), W262S (firebrick), and of K_{2P}1.1 (TWIK-1) (Miller and Long, 2012) (green).

(D) Comparison of indicated channel M4 and M2 helices.

respond to such stimuli, but also should elaborate general principles for how ion channels respond to mechanical and thermal gating input. Determination of the structures of two K_{2P}4.1 (TRAAK) gain-of-function mutants reveals unexpected structural changes in the M4 and M2 transmembrane helices that when taken together with prior K_{2P}4.1 (TRAAK) structures (Brohawn et al., 2012, 2013) reveal a series of molecular transformations that we propose underlie K_{2P} channel activation (Figures 8A–8C). The key conformational changes are: (1) conversion of the M4 helix from a bent to a straight conformation centered on the conserved glycine at K_{2P}4.1 (TRAAK) residue 268, (2) buckling of the M2 helix at the conserved GXG sequence found in all mechanosensitive and thermosensitive K_{2P}s, and (3) the disruption of the M2/M3 interhelix interface caused by the movements of M4 and M2.

The molecular transformation of M4 around the conserved glycine looks very much like the one described from crystallographic studies of the KcsA (Cuello et al., 2010a, 2010b) and KirBac3.1 (Bavro et al., 2012) potassium channels, albeit with one crucial difference. Whereas in these channels the transformation is from a straight helix in the resting state to a bent pore-lining helix in the activated state, the transition in K_{2P}4.1 (TRAAK) appears as the exact opposite: the pore-lining helix is bent at rest, and the activated helix is straight. Unlike other potassium channel classes, K_{2P} channels are not thought to have a closed inner gate that forms a physical barrier to ion passage, but instead rely on a C-type gate at the selectivity filter (Bagriantsev et al., 2011, 2012; Piechotta et al., 2011; Rapedius et al., 2012). The unusual dimeric architecture of K_{2P}s precludes the formation of the convergence of the cytoplasmic ends of the pore-lining helices that would correspond to the classical inner gate seen in other types of channels from this superfamily (Doyle et al., 1998; Payandeh et al., 2011; Shaya et al., 2014; Zhang et al., 2012).

Thus, it appears that free from this constraint, the K_{2P} architecture has been able to harness similar movements, but to opposite functional effects.

Although our structures reveal key transformations in the cytoplasmic portions of the channel, how these changes affect the conformation of the C-type gate remains unclear. Even though there are local changes near the G124I and W262S activating mutants, we were unable to discern any clear changes in the core element of the C-type gate, the selectivity filter. This observation is similar to that made with prior K_{2P}4.1 (TRAAK) structural analysis (Brohawn et al., 2013) and may reflect the limited resolution of the crystallographic data or indicate that the main effects that control the C-type gate are dynamic, rather than strictly structural, or both. It is worth noting that allosteric coupling between a selectivity filter-based gate and movements of the pore-lining helix has been described structurally for C-type inactivation in KcsA (Cuello et al., 2010a, 2010b), and hence, we expect that it should be possible to describe analogous changes in K_{2P}s. Such questions and the details of how a similar M4 movement can lead to opposite outcomes for selectivity filter function will need to be addressed by a combination of higher-resolution structures, functional investigation, and simulation studies.

The asymmetry seen between the subunits in each of the K_{2P}4.1 structures may provide an important clue about how K_{2P}s function. Although the unhindered subunit can adopt a wide range of conformations, in all the structures the subunit that is pinned by crystal lattice interactions near the cytoplasmic side of M2, M3, and M4 shows a conformation that resembles the W262S mutant, which we interpret as an activated state. The ability to trap the M4 helix of subunits engaged in crystal lattice contacts suggests that the energetic barriers for moving this part of the protein are not exceptionally high and must be sampled by the precrystallized state. This concept matches well with the observed behavior of K_{2P}s in response to stimuli. Gating cues cause the activity of these channels to change in a much more gradual manner than the essentially binary modulation associated with channels in which opening the hydrophobic barrier to ion passage formed by the pore-lining helices is the

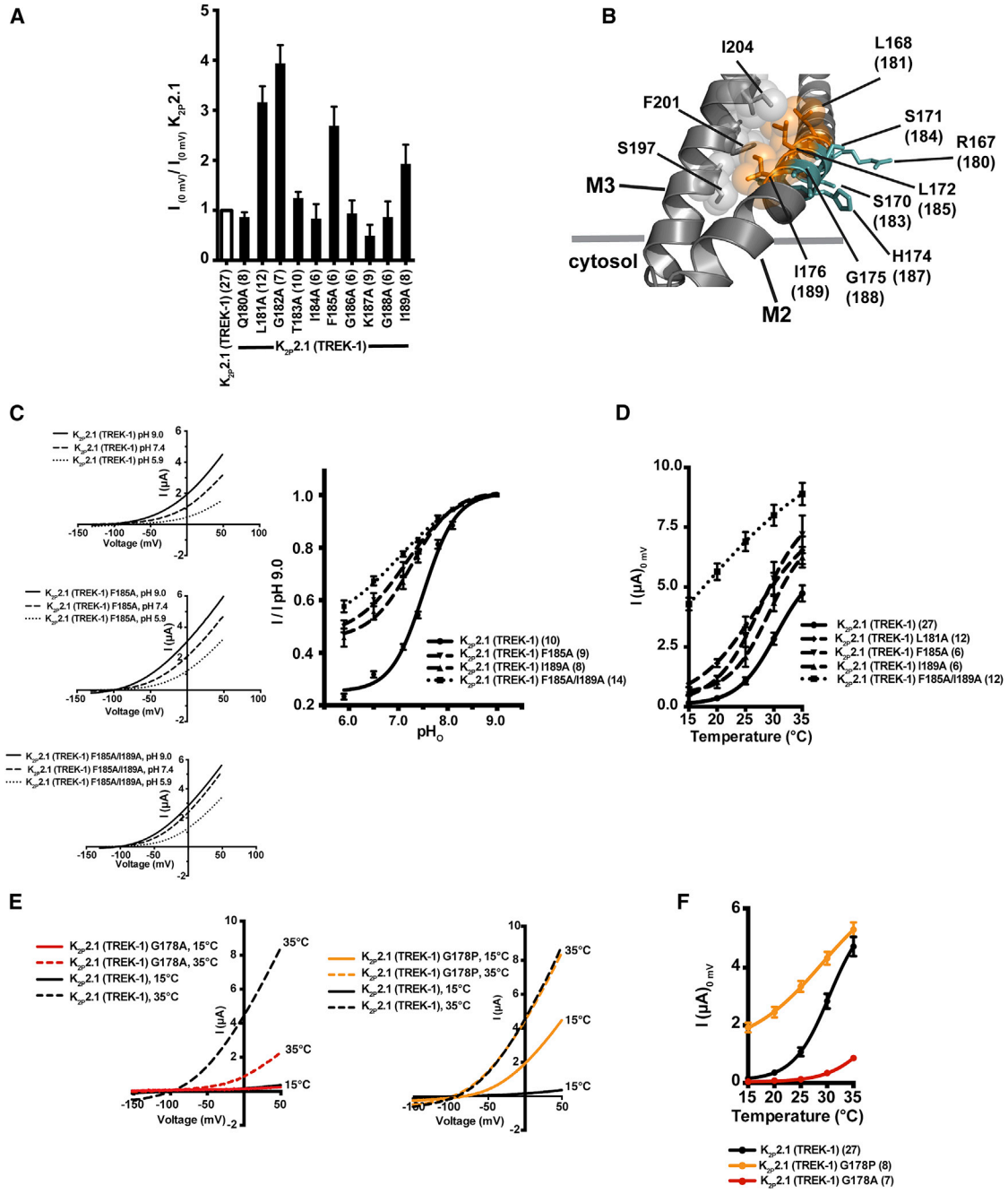

Figure 7. Mutations in the M2/M3 Interface and M2 Buckling Point Activate K_{2P}2.1 (TREK-1) and Affect Thermal Responses

(A) Quantification of normalized current amplitudes measured by two-electrode voltage clamp at 0 mV from *Xenopus* oocytes injected with 1.2 ng of mRNA for the indicated K_{2P}2.1 (TREK-1) channels.

(B) Data from (A) mapped onto the K_{2P}4.1 (TRAAK) M2/M3 interface (Figure 5C). Orange indicates residues for which alanine substitution stimulated basal current. Teal indicates residues in which alanine substation had no effect. K_{2P}2.1 (TREK-1) numbers are shown in parentheses.

(C) Exemplar currents for the indicated channels and normalized pH_O responses (at 0 mV).

(D) Temperature responses at 0 mV for the indicated channels.

(E) Exemplar two-electrode voltage-clamp recordings of the response of K_{2P}2.1 (TREK-1), G178A, and G178P to temperature in 2 mM $[K^+]_O$ (pH 7.4) solutions.

(F) Temperature responses at 0 mV for the indicated channels. Where indicated, parentheses indicate the number of independent measurements. Error bars are mean ± SEM.

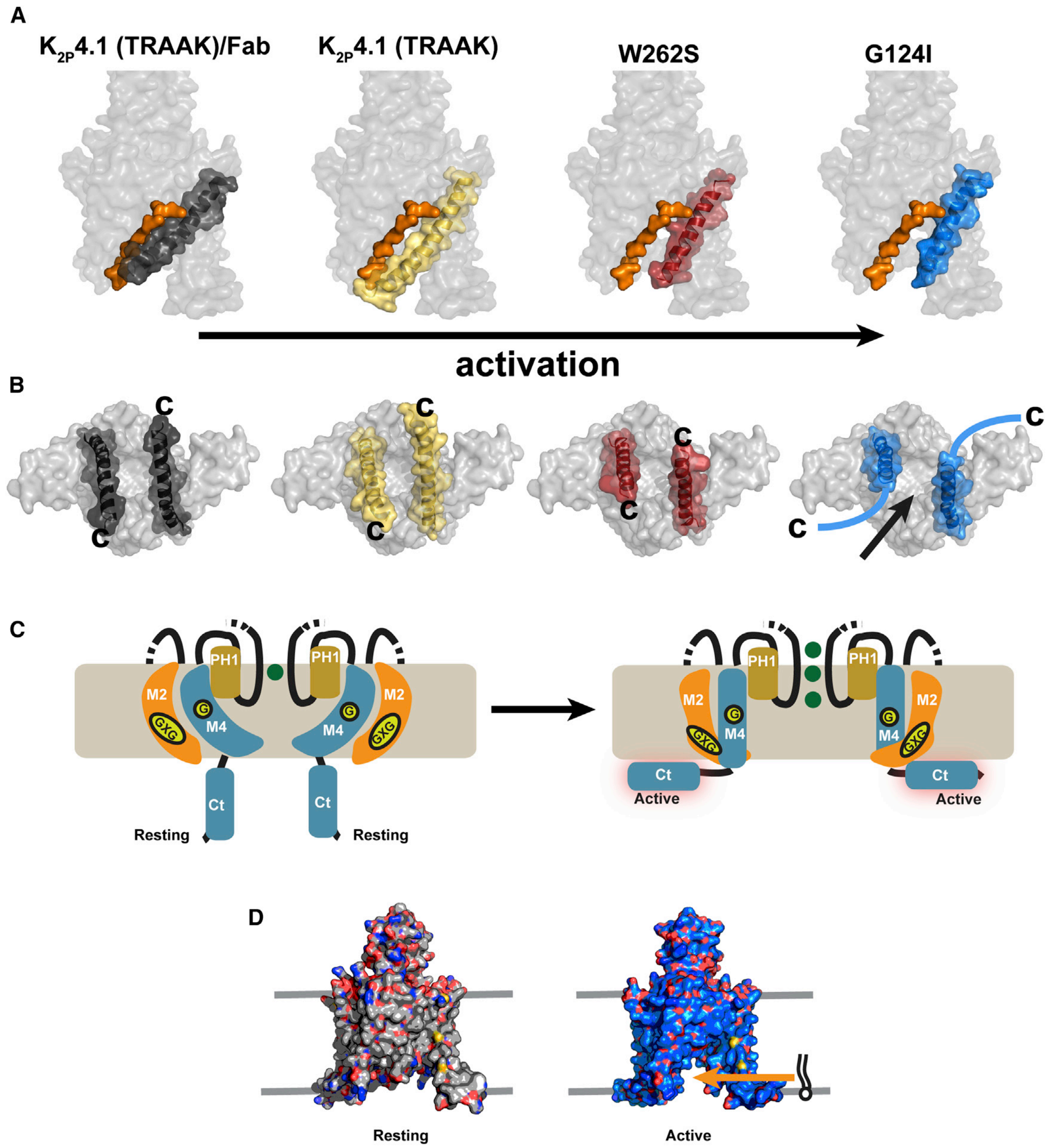

Figure 8. Models of K_{2P} Gating

(A) Proposed activation sequence for mechanosensitive and thermosensitive K_{2P}s. Space-filling models are shown for the structures of the K_{2P}4.1 (TRAAK)/Fab complex (Brohawn et al., 2013), K_{2P}4.1 (TRAAK) (Brohawn et al., 2012), W262S, and G124I. The M2 helix of one subunit is shown in orange. M4 helices are colored as follows: K_{2P}4.1 (TRAAK)/Fab complex (gray), K_{2P}4.1 (TRAAK) (yellow), W262S (firebrick), and G124I (marine).

(B) Structures in (A) viewed from the cytoplasmic face. C-terminal end of M4 is indicated. The lateral door and possible path of the C-terminal tail is indicated for G124I.

(C) Cartoon model of the key K_{2P} moving parts. Conserved M4 glycine and M2 GXG sequences are indicated. Changes in the C-type gate and association of the C-terminal tail with the membrane is based on models from Bagriantsev et al. (2012); Chemin et al. (2005b); and Sandoz et al. (2011).

(D) Space-filling models of the K_{2P}4.1 (TRAAK)/Fab complex (Brohawn et al., 2013) and G124I as models for the resting and activated states, respectively. Possible bilayer boundaries are indicated. Concept of lateral lipid through the lateral door in G124I access is shown.

critical last step for entry into the conductive state. Functional studies using tandem dimer constructs suggest that signals from the main sensor, the cytoplasmic C-terminal domain, are transmitted through M4 to the pore within a single subunit (Bagriantsev et al., 2012). The observed crystallographic asymmetry is very much in line with this notion. Moreover, the observation that interactions at M2/M3/M4 junction affect function suggests that this region may be a target for both natural and designed modulators. Indeed, a number of anesthetics are thought to use elements from this channel region (Andres-Enguix et al.,

2007; Conway and Cotten, 2012; Patel et al., 1999; Talley and Bayliss, 2002). Remarkably, a number of positions corresponding to residues important for channel activation by anesthetics or covalent modification are brought together by the straightening of M4 in the activated conformation (Figure S6). The structural observations made here regarding the M2/M3/M4 conformational changes should focus further investigation on this region.

The cytoplasmic C-terminal tail is a critical sensory element of the K_{2P}4.1 (TRAAK) family members, being involved in temperature (Bagriantsev et al., 2012; Maingret et al., 2000a; Patel et al., 1998), pressure (Chemin et al., 2005b; Honoré et al., 2002; Kim et al., 2001a, 2001b), pH (Honoré et al., 2002), and lipid modulation (Chemin et al., 2005b; Honoré et al., 2002; Kim et al., 2001a, 2001b). This element is not visible in any of the K_{2P}4.1 (TRAAK) structures reported thus far. However, the conformational changes we see in K_{2P}4.1 (TRAAK) G124I and W262S cause a substantial repositioning of the M4 C terminus, which is covalently connected to the tail (Figure 8B; Movie S4). Moreover, the correspondence of the activated position of M4 from G124I and W262S with that of the related channel K_{2P}1.1 (TWIK-1) in which this region is visible in the structure (Miller and Long, 2012) may provide some clues to potential locations of the C-terminal tails. In the G124I and W262S structures, there is a loss of helical structure upon helix straightening that occurs in the same region where the K_{2P}1.1 (TWIK-1) structure transitions into a linker lacking secondary structure that connects M4 with the C-helix and that places the C terminus in the vicinity of the M2/M3 loop. It is striking that two residues implicated in modulation of the related channel K_{2P}2.1 (TREK-1), Ser300, which is the target for phosphorylation that inhibits the channel (Bagriantsev et al., 2012; Murbartián et al., 2005; Segal-Hayoun et al., 2010), and E306A, an activating mutant (Chemin et al., 2005b; Honoré et al., 2002), would be in the vicinity of the M2/M3 loop. Prior studies have suggested that upon activation, the C-terminal tail of K_{2P}2.1 (TREK-1) associates with the bilayer (Chemin et al., 2005b; Sandoz et al., 2008) (Figure 8C). The structural observations about the K_{2P}4.1 (TRAAK) activated state suggest the possibility that this part of the protein may interact with both the bilayer and the protein as part of the activation mechanism.

Structures of a number of channels have revealed the presence of lateral openings to the bilayer from the central channel pore (Brohawn et al., 2012, 2013; McCusker et al., 2012; Miller and Long, 2012; Payandeh et al., 2011, 2012; Shaya et al., 2014; Zhang et al., 2012). Because, as in the structures reported here, there is often evidence of nonprotein electron density in these openings, it has been suggested that such features provide means for hydrophobic modulators, and possibly even lipids, to affect channel function (Brohawn et al., 2012, 2013; Miller and Long, 2012; Nilius and Honoré, 2012; Payandeh et al., 2011, 2012; Payandeh and Minor, 2014; Zhang et al., 2012). The lateral nature of such "windows" to the bilayer is puzzling as it is not clear how much lipids from either portion of the bilayer might have to contort to gain access. In the case of K_{2P}4.1 (TRAAK), the two structures presented here eliminate this problem. The consequence of the large movement caused by the straightening of the M4 helix is that the lateral window that is closed in the most elevated position of M4 (Brohawn et al., 2013) and open in the intermediate M4 pose (Brohawn et al., 2012) becomes a door that appears to face the inner leaflet of the bilayer (Figures 8A and 8D). Such an aperture would allow facile lipid binding for modulators of TRAAK such as AA (Bang et al., 2000; Chemin et al., 2005a, 2005b, 2007; Fink et al., 1998; Maingret et al., 2000b) and PIP_2 (Lopes et al., 2005), as it would only require a lateral movement of the lipid from the inner bilayer leaflet (Figure 8D). This hypothesis is appealing as in such a scenario both the hydrophobic headgroup and fatty acid tails of the lipid could remain in their cognate environments similar to the means by which PIP_2 is thought to interact with Kir3 (GIRK) channels (Whorton and MacKinnon, 2011).

Finally, the distortions of the protein we associate with activated conformations seem to be in line with the general idea that factors such as membrane stretch and elevated temperature will cause structural transitions in the channel protein (Anishkin et al., 2014; Haswell et al., 2011; Kung, 2005; Nilius and Honoré, 2012). The disruption of a small hydrophobic core between M2 and M3 matches the expectation from protein folding studies in which changes of hydrophobic interfaces are central to thermal transitions (Baldwin, 1986; Privalov and Gill, 1988). This apparent convergence of thermal and pressure-induced activation mechanisms suggests that both perturbations rely on similar disruptions in the protein architecture.

EXPERIMENTAL PROCEDURES

Protein Expression and Purification

G124I and W262S mutations were introduced by site-directed mutagenesis into a previously described *P. pastoris* pPICZ vector bearing the human K_{2P}4.1 (TRAAK) (GI:13124080) gene residues 1–300 followed by a C-terminal GFP and His_{10} tag (Brohawn et al., 2012). Plasmids were linearized with *PmeI* and transformed into *P. pastoris* SMD1163 by electroporation. Multi-integration recombinants were selected by plating transformants onto yeast extract peptone dextrose sorbitol (YPDS) plates at increasing concentrations of zeocin (1–4 mg ml^{-1}).

Fluorescence-detection size-exclusion chromatography (FSEC) screening (Drew et al., 2008; Kawate and Gouaux, 2006; Newstead et al., 2007) was used to evaluate expression levels of individual transformants. Ten of the most zeocin-resistant colonies of each mutant were picked and grown in a 10 ml minimal medium (2 × yeast nitrogen base [YNB] [Sigma, #Y0626], 1% glycerol, 0.4 mg L^{-1} biotin, 40 mg L^{-1} L-histidine, 100 mM potassium phosphate [pH 6.0]) to OD_{600} = 10 (~2 days). Methanol was added to a final concentration of 0.5% (v/v). After 24 hr induction, additional methanol (final concentration of 0.5% [v/v]) was added, and the induction continued for another 24 hr. Cells were harvested by centrifugation (3,000 × g at 4°C, 10 min) and resuspended in 1 ml of lysis buffer (150 mM KCl, 1 mM PMSF, 50 mM Tris-Cl [pH 8.0]). A total of 0.3 g of acid-washed glass beads were then added to each sample. Cells were broken by vortexing (3 × 3 min) and centrifuged (100,000 × g at 4°C, 20 min). The pellet was resuspended in 500 μl of solubilization buffer (150 mM KCl, 1 mM PMSF, 60 mM n-dodecyl-β-D-maltopyranoside [DDM], 50 mM Tris-Cl [pH 8.0]) and incubated at 4°C for 1 hr. Debris was removed by centrifugation (100,000 × g at 4°C, 30 min), and the supernatant was loaded onto a Superose 6 column (GE Healthcare, 10/300 GL) equilibrated with FSEC buffer (150 mM KCl, 1.5 mM DDM, 20 mM Tris-Cl [pH 8.0]) and connected to an auto sampler (Shimadzu, SIL-20AHT/20ACHT) and in-line fluorescence detector (Shimadzu, RF-10A). Fluorescence profile of each clone (485 nm excitation/540 nm emission) was compared. Clones with the highest fluorescence intensity and narrowest, most symmetric peak were chosen for large-scale growth.

For large-scale expression, a 120 ml starting culture was grown in buffered minimal medium (2 × YNB, 1% glycerol, 0.4 mg L^{-1} biotin, 40 mg L^{-1} L-histidine, 100 mM potassium phosphate [pH 6.0]) for 2 days at 29°C and used at a

ratio of 1/100 to inoculate twelve 2.8 L flasks containing 1 L each of buffered minimal medium. Cells were grown on a shaker (29°C, 235 rpm) for 2 days, harvested by centrifugation (3,000 × g at 20°C, 6 min), and resuspended in fresh minimal medium in which the glycerol was replaced by 0.5% (v/v) methanol to induce expression. After 24 hr, additional methanol was added (final concentration 0.5% [v/v]) to the culture. Cells were pelleted by centrifugation (6,000 × g at 4°C for 30 min) 48 hr after initial induction, snap frozen in liquid nitrogen, and stored at −80°C.

Cells were broken by cryomilling (Retsch model MM400) in liquid nitrogen (3 × 3 min, 25 Hz). In between each milling step the canisters were placed in liquid nitrogen to cool. All subsequent purification was carried out at 4°C. Cell powder was added at a ratio of 1 g cell powder/4 ml lysis buffer (150 mM KCl, 60 mM DDM, 0.1 mg mL^{-1} DNase, 1 mM PMSF, 100 mM Tris-Cl [pH 8.2], and 1 tablet/50 ml of EDTA-free complete inhibitor cocktail [Roche]). Membranes were extracted as previously reported (Brohawn et al., 2012) for 3 hr with gentle stirring followed by centrifugation (100,000 × g at 4°C, 45 min).

Solubilized proteins were purified by affinity chromatography using batch purification. Talon cobalt resin (Clontech Laboratories, #635503) was added to the supernatant at a ratio of 1 ml of resin per 10 g of cell powder and incubated overnight at 4°C with gentle shaking. Resin was collected into a column and washed with four column volumes (CVs) of buffer A (150 mM KCl, 6 mM DDM, 10 mM imidazole, 50 mM Tris [pH 8.0]) followed by a second wash step using four CVs of buffer A containing 20 mM imidazole (pH 8.0). Bound protein was then eluted using four CVs of buffer A containing 500 mM imidazole (pH 8.0).

Affinity column eluate was supplemented to contain 350 mM KCl and 1 mM EDTA. To remove the affinity tag, 3C protease (Shaya et al., 2011) was added at a ratio of 10:1 (wt/wt) fusion protein:protease and incubated with gentle rocking overnight at 4°C. Protein concentration was determined by UV absorbance at 280 nm in native buffer, using the extinction coefficient of the fusion protein (ε = 61,497 M^{-1} cm^{-1} and ε = 66,997 M^{-1} cm^{-1} for W262S and G124I, respectively). The resulting mixture was applied to a desalting column (HiPrep 26/10, GE Healthcare, #17-5087-01) using buffer B as eluent (10 mM KCl, 2 mM DDM, 50 mM Tris-Cl [pH 8.0]). Desalted sample was applied to an anion-exchange column (8 ml POROS 50 HQ, #1-2559-11) and eluted with a linear gradient to 500 mM KCl over 35 CVs. Fractions containing the protein were pooled, concentrated, and applied to a Superdex 200 column equilibrated in buffer C (150 mM KCl, 1 mM DDM, 1 mM EDTA, 20 mM Tris-Cl [pH 8.0]).

Crystallization and Structure Determination

Purified W262S and G124I were concentrated to 10–13 mg ml^{-1} by centrifugation (Amicon Ultra-15, 50 kDa molecular mass cutoff; Millipore) and crystallized by hanging-drop vapor diffusion at 4°C using a mixture of 0.4 μl of protein and 0.9 μl of precipitant. W262S crystals grew over a reservoir of 24% PEG400 and 10 mM sarcosine. Crystals were cryoprotected with 30% PEG400, 10 mM sarcosine in buffer C, and flash frozen in liquid nitrogen. G124I crystallized over a reservoir of 23% PEG400, 2% PEG3350. Crystals were harvested and moved to a 3 μl drop containing 25% PEG400, 30% PEG3350, 1 mM Fos-choline-12 in buffer C, and incubated for 1 min at 4°C before plunging them in liquid nitrogen. In both cases, crystals were visible after 4 days and grew to full size (100 μm × 50 μm × 15 μm) after 1 week.

Multiple full data sets (12 for G124I and 14 for W262S mutant) were collected at 100K using synchrotron radiation (APS GM/CAT beamline 23-IDB, Chicago), processed with XDS (Kabsch, 2010), analyzed with *BLEND* (Foadi et al., 2013), and scaled and merged with Aimless (Evans and Murshudov, 2013). Final resolution cutoff was 3.4Å and 3.3Å for W262S and G124I, respectively, using the $CC_{1/2}$ criterion (Diederichs and Karplus, 2013; Karplus and Diederichs, 2012). Structures were solved by molecular replacement using only the channel portion of PDB 4I9W as search model. Several cycles of manual rebuilding, using COOT (Emsley and Cowtan, 2004), and refinement using REFMAC5 (Collaborative Computational Project, Number 4, 1994) and PHENIX (Adams et al., 2010), were carried out to improve the electron density map. Two-fold local medium noncrystallographic symmetry (NCS) restraints were employed during refinement for residues 28–103, 110–158, and 194–260. NCS restraints were released in the final round of refinement.

Patch-Clamp Electrophysiology

The sequence coding for human K_{2P}4.1 (TRAAK) (hK_{2P}4.1 (TRAAK); GI:13124080) was subcloned into pIRES2-EGFP for mammalian expression. HEK293T cells were transfected (in 35 mm diameter wells) with LipofectAMINE 2000 (Invitrogen) and plated onto coverslips coated with Matrigel (BD Biosciences).

The effects of AA and stretch activation were characterized as previously described (Maingret et al., 1999a). Effects of AA and ML67-33 activation on hK_{2P}4.1 (TRAAK), W262S, and G124I were measured by whole-cell patch-clamp experiments 24 hr after transfection. Acquisition and analysis were performed using pCLAMP9 and an Axopatch 200B amplifier (Molecular Devices). The pipette resistance ranged from 1 to 2.5 MΩ. Series resistance was compensated by 60%–80%. Pipette solution contained the following, in millimolars: 145, KCl; 3, $MgCl_2$; 5, EGTA; 20, HEPES (pH 7.2 with KOH). Bath solution contained the following, in millimolars: 145, NaCl; 5, KCl; 1, $CaCl_2$; 3, $MgCl_2$; 20, HEPES (pH 7.4 with NaOH). K_{2P}4.1 (TRAAK) currents were elicited by a 1 s ramp from −100 to +50 mV from a −80 mV holding potential. After stabilization of the basal current, AA and ML67-33 were perfused at 200 ml hr^{-1} until the potentiation was stably reached.

Stretch activation of hK_{2P}4.1 (TRAAK), G124I, and W262S was performed on excised patches in the inside-out configuration. A −50 mm Hg pressure was applied to the patch through a High-Speed Pressure Clamp (HSPC-1, ALA Scientific Instruments) connected to the electrode suction port after recording the current at 0 mm Hg. Basal current was ≥ 500 pA. Pipette solution contained the following in millimolars: 150, NaCl; 5, KCl; 1, $CaCl_2$; 2, $MgCl_2$; 20, HEPES (pH 7.4 with NaOH). Bath solution contained the following in millimolars: 145, KCl; 3, $MgCl_2$; 5, EGTA; 20 HEPES (pH 7.2 with KOH) and was continuously perfused at 200 ml hr^{-1} during the experiment. hK_{2P}4.1 (TRAAK) currents were elicited by a 1 s ramp from −150 to +50 mV from a −80 mV holding potential. Data were analyzed using Clampfit 9 and Origin 7.

Two-Electrode Voltage Clamp Electrophysiology

Two-electrode voltage clamp recordings were performed on defolliculated stage V–VI *Xenopus laevis* oocytes 24–48 hr after microinjection with 1.2 ng cRNA. Surgical extraction of *Xenopus* oocytes was done under an IACUC-approved protocol. Oocytes were impaled with borosilicate recording microelectrodes (0.3–3.0 MΩ resistance) backfilled with 3 M KCl. Recording solution (96 mM NaCl, 2 mM KCl, 1.8 mM $CaCl_2$, and 2.0 mM $MgCl_2$, buffered with 5 mM HEPES [pH 7.4]) was perfused at a rate of 3 ml min^{-1}. For pH_O experiments, 5 mM HEPES was replaced by 10 mM TRIS (pH 9.0, 8.1) or 5 mM MES (pH 6.5, 5.9) as indicated in the text. For temperature experiments, recording solutions were heated by an SC-20 in-line heater/cooler combined with an LCS-1 liquid cooling system operated by the CL-100 bipolar temperature controller (Warner Instruments). Temperature was monitored using a CL-100-controlled thermistor placed in the bath solution 1 mm upstream of the oocyte. For pH experiments, solutions were exchanged sequentially from pH 9.0 to pH 5.9, and recordings were performed 15 s after each new solution was applied, as described previously (Bagriantsev et al., 2011). For temperature experiments, perfusate was warmed from 15°C to 35°C in 5°C increments, with recordings performed once temperature readings stabilized at the desired values. Currents were evoked from a −80 mV holding potential by a 100 ms step to 0 mV, a 100 ms return to −80mV, followed by a 500 ms ramp from −150 mV to +50 mV. Data were acquired using a GeneClamp 500B amplifier (MDS Analytical Technologies) controlled by pClamp software (Molecular Devices), and digitized at 1 kHz using Digidata 1332A digitizer (MDS Analytical Technologies). Aggregate pH_O data were fitted with a modified Hill equation: $I = I_{min}+(I_{max}-I_{min})/(1+10\text{^}((pH_OIC_{50}/pH_O)*H))$, where I_{max} and I_{min} are maximal and minimal current values, respectively, $pHoIC_{50}$ is a half-maximal effective pH_O value, and H is the Hill coefficient.

ACCESSION NUMBERS

The Protein Data Bank accession numbers for coordinates and structure factors for G124I and W262S reported in this paper are 4RUE and 4RUF, respectively.

SUPPLEMENTAL INFORMATION

Supplemental Information includes six figures, one table, and four movies and can be found with this article online at http://dx.doi.org/10.1016/j.neuron.2014.11.017.

AUTHOR CONTRIBUTIONS

M.L., C.A., P.M.R., and D.L.M. conceived the study and designed the experiments. M.L. purified and crystallized the proteins, collected diffraction data, and determined, refined, and analyzed the structures. C.A. and P.M.R. designed and performed functional experiments in HEK cells and *Xenopus* oocytes, respectively. K.A.C. expressed and purified the proteins. D.L.M. analyzed data and provided guidance and support throughout. M.L., C.A., P.M.R., and D.L.M. wrote the paper.

ACKNOWLEDGMENTS

We thank S. Brohawn and R. MacKinnon (Rockefeller University) for the K_{2P}4.1 (TRAAK) plasmid; F. Findeisen for expert advice on structure solution and refinement; and S.N. Bagriantsev, J.M. Berger, K. Brejc, M. Grabe, J. Gross, L. Jan, J. Payandeh, and E. Reuveny for comments on the manuscript. This work was supported by NIH-NIMH grant R01-MH093603 to D.L.M.

Accepted: November 20, 2014
Published: December 10, 2014

REFERENCES

Adams, P.D., Afonine, P.V., Bunkóczi, G., Chen, V.B., Davis, I.W., Echols, N., Headd, J.J., Hung, L.W., Kapral, G.J., Grosse-Kunstleve, R.W., et al. (2010). PHENIX: a comprehensive Python-based system for macromolecular structure solution. Acta Crystallogr. D Biol. Crystallogr. *66*, 213–221.

Alloui, A., Zimmermann, K., Mamet, J., Duprat, F., Noël, J., Chemin, J., Guy, N., Blondeau, N., Voilley, N., Rubat-Coudert, C., et al. (2006). TREK-1, a K+ channel involved in polymodal pain perception. EMBO J. *25*, 2368–2376.

Andres-Enguix, I., Caley, A., Yustos, R., Schumacher, M.A., Spanu, P.D., Dickinson, R., Maze, M., and Franks, N.P. (2007). Determinants of the anesthetic sensitivity of two-pore domain acid-sensitive potassium channels: molecular cloning of an anesthetic-activated potassium channel from *Lymnaea stagnalis*. J. Biol. Chem. *282*, 20977–20990.

Anishkin, A., Loukin, S.H., Teng, J., and Kung, C. (2014). Feeling the hidden mechanical forces in lipid bilayer is an original sense. Proc. Natl. Acad. Sci. USA *111*, 7898–7905.

Bagriantsev, S.N., Peyronnet, R., Clark, K.A., Honoré, E., and Minor, D.L., Jr. (2011). Multiple modalities converge on a common gate to control K2P channel function. EMBO J. *30*, 3594–3606.

Bagriantsev, S.N., Clark, K.A., and Minor, D.L., Jr. (2012). Metabolic and thermal stimuli control K(2P)2.1 (TREK-1) through modular sensory and gating domains. EMBO J. *31*, 3297–3308.

Bagriantsev, S.N., Ang, K.H., Gallardo-Godoy, A., Clark, K.A., Arkin, M.R., Renslo, A.R., and Minor, D.L., Jr. (2013). A high-throughput functional screen identifies small molecule regulators of temperature- and mechano-sensitive K2P channels. ACS Chem. Biol. *8*, 1841–1851.

Bagriantsev, S.N., Gracheva, E.O., and Gallagher, P.G. (2014). Piezo proteins: regulators of mechanosensation and other cellular processes. J. Biol. Chem. *289*, 31673–31681.

Baldwin, R.L. (1986). Temperature dependence of the hydrophobic interaction in protein folding. Proc. Natl. Acad. Sci. USA *83*, 8069–8072.

Bandell, M., Macpherson, L.J., and Patapoutian, A. (2007). From chills to chilis: mechanisms for thermosensation and chemesthesis via thermoTRPs. Curr. Opin. Neurobiol. *17*, 490–497.

Bang, H., Kim, Y., and Kim, D. (2000). TREK-2, a new member of the mechanosensitive tandem-pore K+ channel family. J. Biol. Chem. *275*, 17412–17419.

Bavro, V.N., De Zorzi, R., Schmidt, M.R., Muniz, J.R., Zubcevic, L., Sansom, M.S., Vénien-Bryan, C., and Tucker, S.J. (2012). Structure of a KirBac potassium channel with an open bundle crossing indicates a mechanism of channel gating. Nat. Struct. Mol. Biol. *19*, 158–163.

Brohawn, S.G., del Mármol, J., and MacKinnon, R. (2012). Crystal structure of the human K2P TRAAK, a lipid- and mechano-sensitive K+ ion channel. Science *335*, 436–441.

Brohawn, S.G., Campbell, E.B., and MacKinnon, R. (2013). Domain-swapped chain connectivity and gated membrane access in a Fab-mediated crystal of the human TRAAK K+ channel. Proc. Natl. Acad. Sci. USA *110*, 2129–2134.

Brohawn, S.G., Su, Z., and MacKinnon, R. (2014). Mechanosensitivity is mediated directly by the lipid membrane in TRAAK and TREK1 K+ channels. Proc. Natl. Acad. Sci. USA *111*, 3614–3619.

Cao, E., Liao, M., Cheng, Y., and Julius, D. (2013). TRPV1 structures in distinct conformations reveal activation mechanisms. Nature *504*, 113–118.

Chemin, J., Patel, A., Duprat, F., Zanzouri, M., Lazdunski, M., and Honoré, E. (2005a). Lysophosphatidic acid-operated K+ channels. J. Biol. Chem. *280*, 4415–4421.

Chemin, J., Patel, A.J., Duprat, F., Lauritzen, I., Lazdunski, M., and Honoré, E. (2005b). A phospholipid sensor controls mechanogating of the K+ channel TREK-1. EMBO J. *24*, 44–53.

Chemin, J., Patel, A.J., Duprat, F., Sachs, F., Lazdunski, M., and Honore, E. (2007). Up- and down-regulation of the mechano-gated K(2P) channel TREK-1 by PIP (2) and other membrane phospholipids. Pflugers Arch. *455*, 97–103.

Chowdhury, S., Jarecki, B.W., and Chanda, B. (2014). A molecular framework for temperature-dependent gating of ion channels. Cell *158*, 1148–1158.

Clapham, D.E., and Miller, C. (2011). A thermodynamic framework for understanding temperature sensing by transient receptor potential (TRP) channels. Proc. Natl. Acad. Sci. USA *108*, 19492–19497.

Clarke, C.E., Veale, E.L., Wyse, K., Vandenberg, J.I., and Mathie, A. (2008). The M1P1 loop of TASK3 K2P channels apposes the selectivity filter and influences channel function. J. Biol. Chem. *283*, 16985–16992.

Cohen, A., Ben-Abu, Y., Hen, S., and Zilberberg, N. (2008). A novel mechanism for human K2P2.1 channel gating. Facilitation of C-type gating by protonation of extracellular histidine residues. J. Biol. Chem. *283*, 19448–19455.

Collaborative Computational Project, Number 4 (1994). The CCP4 suite: programs for protein crystallography. Acta Crystallogr. D Biol. Crystallogr. *50*, 760–763.

Conway, K.E., and Cotten, J.F. (2012). Covalent modification of a volatile anesthetic regulatory site activates TASK-3 (KCNK9) tandem-pore potassium channels. Mol. Pharmacol. *81*, 393–400.

Cordes, F.S., Bright, J.N., and Sansom, M.S. (2002). Proline-induced distortions of transmembrane helices. J. Mol. Biol. *323*, 951–960.

Cuello, L.G., Jogini, V., Cortes, D.M., Pan, A.C., Gagnon, D.G., Dalmas, O., Cordero-Morales, J.F., Chakrapani, S., Roux, B., and Perozo, E. (2010a). Structural basis for the coupling between activation and inactivation gates in K(+) channels. Nature *466*, 272–275.

Cuello, L.G., Jogini, V., Cortes, D.M., and Perozo, E. (2010b). Structural mechanism of C-type inactivation in K(+) channels. Nature *466*, 203–208.

Dedman, A., Sharif-Naeini, R., Folgering, J.H., Duprat, F., Patel, A., and Honoré, E. (2009). The mechano-gated K(2P) channel TREK-1. Eur. Biophys. J. *38*, 293–303.

Diederichs, K., and Karplus, P.A. (2013). Better models by discarding data? Acta Crystallogr. D Biol. Crystallogr. *69*, 1215–1222.

Doyle, D.A., Morais Cabral, J., Pfuetzner, R.A., Kuo, A., Gulbis, J.M., Cohen, S.L., Chait, B.T., and MacKinnon, R. (1998). The structure of the potassium channel: molecular basis of K^+ conduction and selectivity. Science *280*, 69–77.

Drew, D., Newstead, S., Sonoda, Y., Kim, H., von Heijne, G., and Iwata, S. (2008). GFP-based optimization scheme for the overexpression and purification of eukaryotic membrane proteins in *Saccharomyces cerevisiae*. Nat. Protoc. *3*, 784–798.

Emsley, P., and Cowtan, K. (2004). Coot: model-building tools for molecular graphics. Acta Crystallogr. D Biol. Crystallogr. *60*, 2126–2132.

Enyedi, P., and Czirják, G. (2010). Molecular background of leak K+ currents: two-pore domain potassium channels. Physiol. Rev. *90*, 559–605.

Evans, P.R., and Murshudov, G.N. (2013). How good are my data and what is the resolution? Acta Crystallogr. D Biol. Crystallogr. *69*, 1204–1214.

Faham, S., Yang, D., Bare, E., Yohannan, S., Whitelegge, J.P., and Bowie, J.U. (2004). Side-chain contributions to membrane protein structure and stability. J. Mol. Biol. *335*, 297–305.

Fink, M., Duprat, F., Lesage, F., Reyes, R., Romey, G., Heurteaux, C., and Lazdunski, M. (1996). Cloning, functional expression and brain localization of a novel unconventional outward rectifier K+ channel. EMBO J. *15*, 6854–6862.

Fink, M., Lesage, F., Duprat, F., Heurteaux, C., Reyes, R., Fosset, M., and Lazdunski, M. (1998). A neuronal two P domain K^+ channel stimulated by arachidonic acid and polyunsaturated fatty acids. EMBO J. *17*, 3297–3308.

Foadi, J., Aller, P., Alguel, Y., Cameron, A., Axford, D., Owen, R.L., Armour, W., Waterman, D.G., Iwata, S., and Evans, G. (2013). Clustering procedures for the optimal selection of data sets from multiple crystals in macromolecular crystallography. Acta Crystallogr. D Biol. Crystallogr. *69*, 1617–1632.

Haswell, E.S., Phillips, R., and Rees, D.C. (2011). Mechanosensitive channels: what can they do and how do they do it? Structure *19*, 1356–1369.

Honoré, E. (2007). The neuronal background K2P channels: focus on TREK1. Nat. Rev. Neurosci. *8*, 251–261.

Honoré, E., Maingret, F., Lazdunski, M., and Patel, A.J. (2002). An intracellular proton sensor commands lipid- and mechano-gating of the K(+) channel TREK-1. EMBO J. *21*, 2968–2976.

Jiang, Y., Lee, A., Chen, J., Cadene, M., Chait, B.T., and MacKinnon, R. (2002). The open pore conformation of potassium channels. Nature *417*, 523–526.

Jordt, S.E., McKemy, D.D., and Julius, D. (2003). Lessons from peppers and peppermint: the molecular logic of thermosensation. Curr. Opin. Neurobiol. *13*, 487–492.

Julius, D. (2013). TRP channels and pain. Annu. Rev. Cell Dev. Biol. *29*, 355–384.

Kabsch, W. (2010). Xds. Acta Crystallogr. D Biol. Crystallogr. *66*, 125–132.

Kamajaya, A., Kaiser, J.T., Lee, J., Reid, M., and Rees, D.C. (2014). The structure of a conserved Piezo channel domain reveals a topologically distinct β sandwich fold. Structure *22*, 1520–1527.

Kang, D., Choe, C., and Kim, D. (2005). Thermosensitivity of the two-pore domain K+ channels TREK-2 and TRAAK. J. Physiol. *564*, 103–116.

Karplus, P.A., and Diederichs, K. (2012). Linking crystallographic model and data quality. Science *336*, 1030–1033.

Kawate, T., and Gouaux, E. (2006). Fluorescence-detection size-exclusion chromatography for precrystallization screening of integral membrane proteins. Structure *14*, 673–681.

Kim, Y., Bang, H., Gnatenco, C., and Kim, D. (2001a). Synergistic interaction and the role of C-terminus in the activation of TRAAK K+ channels by pressure, free fatty acids and alkali. Pflugers Arch. *442*, 64–72.

Kim, Y., Gnatenco, C., Bang, H., and Kim, D. (2001b). Localization of TREK-2 K+ channel domains that regulate channel kinetics and sensitivity to pressure, fatty acids and pHi. Pflugers Arch. *442*, 952–960.

Kung, C. (2005). A possible unifying principle for mechanosensation. Nature *436*, 647–654.

Kung, C., Martinac, B., and Sukharev, S. (2010). Mechanosensitive channels in microbes. Annu. Rev. Microbiol. *64*, 313–329.

Lesage, F., and Barhanin, J. (2011). Molecular physiology of pH-sensitive background K(2P) channels. Physiology (Bethesda) *26*, 424–437.

Lesage, F., Maingret, F., and Lazdunski, M. (2000a). Cloning and expression of human TRAAK, a polyunsaturated fatty acids-activated and mechano-sensitive K(+) channel. FEBS Lett. *471*, 137–140.

Lesage, F., Terrenoire, C., Romey, G., and Lazdunski, M. (2000b). Human TREK2, a 2P domain mechano-sensitive K+ channel with multiple regulations by polyunsaturated fatty acids, lysophospholipids, and Gs, Gi, and Gq protein-coupled receptors. J. Biol. Chem. *275*, 28398–28405.

Liao, M., Cao, E., Julius, D., and Cheng, Y. (2013). Structure of the TRPV1 ion channel determined by electron cryo-microscopy. Nature *504*, 107–112.

Lopes, C.M., Gallagher, P.G., Buck, M.E., Butler, M.H., and Goldstein, S.A. (2000). Proton block and voltage gating are potassium-dependent in the cardiac leak channel Kcnk3. J. Biol. Chem. *275*, 16969–16978.

Lopes, C.M., Rohács, T., Czirják, G., Balla, T., Enyedi, P., and Logothetis, D.E. (2005). PIP2 hydrolysis underlies agonist-induced inhibition and regulates voltage gating of two-pore domain K+ channels. J. Physiol. *564*, 117–129.

Magidovich, E., and Yifrach, O. (2004). Conserved gating hinge in ligand- and voltage-dependent K+ channels. Biochemistry *43*, 13242–13247.

Maingret, F., Fosset, M., Lesage, F., Lazdunski, M., and Honoré, E. (1999a). TRAAK is a mammalian neuronal mechano-gated K^+ channel. J. Biol. Chem. *274*, 1381–1387.

Maingret, F., Patel, A.J., Lesage, F., Lazdunski, M., and Honoré, E. (1999b). Mechano- or acid stimulation, two interactive modes of activation of the TREK-1 potassium channel. J. Biol. Chem. *274*, 26691–26696.

Maingret, F., Lauritzen, I., Patel, A.J., Heurteaux, C., Reyes, R., Lesage, F., Lazdunski, M., and Honoré, E. (2000a). TREK-1 is a heat-activated background K(+) channel. EMBO J. *19*, 2483–2491.

Maingret, F., Patel, A.J., Lesage, F., Lazdunski, M., and Honoré, E. (2000b). Lysophospholipids open the two-pore domain mechano-gated K(+) channels TREK-1 and TRAAK. J. Biol. Chem. *275*, 10128–10133.

Mathie, A., Al-Moubarak, E., and Veale, E.L. (2010). Gating of two pore domain potassium channels. J. Physiol. *588*, 3149–3156.

McCusker, E.C., Bagnéris, C., Naylor, C.E., Cole, A.R., D'Avanzo, N., Nichols, C.G., and Wallace, B.A. (2012). Structure of a bacterial voltage-gated sodium channel pore reveals mechanisms of opening and closing. Nat. Commun. *3*, 1102.

Miller, A.N., and Long, S.B. (2012). Crystal structure of the human two-pore domain potassium channel K2P1. Science *335*, 432–436.

Murbartián, J., Lei, Q., Sando, J.J., and Bayliss, D.A. (2005). Sequential phosphorylation mediates receptor- and kinase-induced inhibition of TREK-1 background potassium channels. J. Biol. Chem. *280*, 30175–30184.

Newstead, S., Kim, H., von Heijne, G., Iwata, S., and Drew, D. (2007). High-throughput fluorescent-based optimization of eukaryotic membrane protein overexpression and purification in *Saccharomyces cerevisiae*. Proc. Natl. Acad. Sci. USA *104*, 13936–13941.

Niemeyer, M.I., Cid, L.P., Peña-Münzenmayer, G., and Sepúlveda, F.V. (2010). Separate gating mechanisms mediate the regulation of K2P potassium channel TASK-2 by intra- and extracellular pH. J. Biol. Chem. *285*, 16467–16475.

Nilius, B., and Honoré, E. (2012). Sensing pressure with ion channels. Trends Neurosci. *35*, 477–486.

Noël, J., Zimmermann, K., Busserolles, J., Deval, E., Alloui, A., Diochot, S., Guy, N., Borsotto, M., Reeh, P., Eschalier, A., and Lazdunski, M. (2009). The mechano-activated K+ channels TRAAK and TREK-1 control both warm and cold perception. EMBO J. *28*, 1308–1318.

Noël, J., Sandoz, G., and Lesage, F. (2011). Molecular regulations governing TREK and TRAAK channel functions. Channels (Austin) *5*, 402–409.

Patel, A.J., Honoré, E., Maingret, F., Lesage, F., Fink, M., Duprat, F., and Lazdunski, M. (1998). A mammalian two pore domain mechano-gated S-like K+ channel. EMBO J. *17*, 4283–4290.

Patel, A.J., Honoré, E., Lesage, F., Fink, M., Romey, G., and Lazdunski, M. (1999). Inhalational anesthetics activate two-pore-domain background K+ channels. Nat. Neurosci. *2*, 422–426.

Payandeh, J., and Minor, D.L., Jr. (2014). Bacterial voltage-gated sodium channels (BacNaVs) from the soil, sea, and salt lakes enlighten molecular mechanisms of electrical signaling and pharmacology in the brain and heart. J. Mol. Biol. Published online August 23, 2014. http://dx.doi.org/10.1016/j.jmb.2014.08.010.

Payandeh, J., Scheuer, T., Zheng, N., and Catterall, W.A. (2011). The crystal structure of a voltage-gated sodium channel. Nature *475*, 353–358.

Payandeh, J., Gamal El-Din, T.M., Scheuer, T., Zheng, N., and Catterall, W.A. (2012). Crystal structure of a voltage-gated sodium channel in two potentially inactivated states. Nature *486*, 135–139.

Pereira, V., Busserolles, J., Christin, M., Devilliers, M., Poupon, L., Legha, W., Alloui, A., Aissouni, Y., Bourinet, E., Lesage, F., et al. (2014). Role of the TREK2 potassium channel in cold and warm thermosensation and in pain perception. Pain. Published online September 18, 2014. http://dx.doi.org/10.1016/j.pain.2014.09.013.

Piechotta, P.L., Rapedius, M., Stansfeld, P.J., Bollepalli, M.K., Ehrlich, G., Andres-Enguix, I., Fritzenschaft, H., Decher, N., Sansom, M.S., Tucker, S.J., and Baukrowitz, T. (2011). The pore structure and gating mechanism of K2P channels. EMBO J. *30*, 3607–3619.

Privalov, P.L., and Gill, S.J. (1988). Stability of protein structure and hydrophobic interaction. Adv. Protein Chem. *39*, 191–234.

Rapedius, M., Schmidt, M.R., Sharma, C., Stansfeld, P.J., Sansom, M.S., Baukrowitz, T., and Tucker, S.J. (2012). State-independent intracellular access of quaternary ammonium blockers to the pore of TREK-1. Channels (Austin) *6*, 473–478.

Sandoz, G., Tardy, M.P., Thümmler, S., Feliciangeli, S., Lazdunski, M., and Lesage, F. (2008). Mtap2 is a constituent of the protein network that regulates twik-related K+ channel expression and trafficking. J. Neurosci. *28*, 8545–8552.

Sandoz, G., Bell, S.C., and Isacoff, E.Y. (2011). Optical probing of a dynamic membrane interaction that regulates the TREK1 channel. Proc. Natl. Acad. Sci. USA *108*, 2605–2610.

Segal-Hayoun, Y., Cohen, A., and Zilberberg, N. (2010). Molecular mechanisms underlying membrane-potential-mediated regulation of neuronal K2P2.1 channels. Mol. Cell. Neurosci. *43*, 117–126.

Shaya, D., Kreir, M., Robbins, R.A., Wong, S., Hammon, J., Brüggemann, A., and Minor, D.L., Jr. (2011). Voltage-gated sodium channel (NaV) protein dissection creates a set of functional pore-only proteins. Proc. Natl. Acad. Sci. USA *108*, 12313–12318.

Shaya, D., Findeisen, F., Abderemane-Ali, F., Arrigoni, C., Wong, S., Nurva, S.R., Loussouarn, G., and Minor, D.L., Jr. (2014). Structure of a prokaryotic sodium channel pore reveals essential gating elements and an outer ion binding site common to eukaryotic channels. J. Mol. Biol. *426*, 467–483.

Talley, E.M., and Bayliss, D.A. (2002). Modulation of TASK-1 (Kcnk3) and TASK-3 (Kcnk9) potassium channels: volatile anesthetics and neurotransmitters share a molecular site of action. J. Biol. Chem. *277*, 17733–17742.

Tsunozaki, M., and Bautista, D.M. (2009). Mammalian somatosensory mechanotransduction. Curr. Opin. Neurobiol. *19*, 362–369.

Uysal, S., Vásquez, V., Tereshko, V., Esaki, K., Fellouse, F.A., Sidhu, S.S., Koide, S., Perozo, E., and Kossiakoff, A. (2009). Crystal structure of full-length KcsA in its closed conformation. Proc. Natl. Acad. Sci. USA *106*, 6644–6649.

Vay, L., Gu, C., and McNaughton, P.A. (2012). The thermo-TRP ion channel family: properties and therapeutic implications. Br. J. Pharmacol. *165*, 787–801.

Vriens, J., Nilius, B., and Voets, T. (2014). Peripheral thermosensation in mammals. Nat. Rev. Neurosci. *15*, 573–589.

Whorton, M.R., and MacKinnon, R. (2011). Crystal structure of the mammalian GIRK2 K+ channel and gating regulation by G proteins, PIP2, and sodium. Cell *147*, 199–208.

Yohannan, S., Faham, S., Yang, D., Whitelegge, J.P., and Bowie, J.U. (2004a). The evolution of transmembrane helix kinks and the structural diversity of G protein-coupled receptors. Proc. Natl. Acad. Sci. USA *101*, 959–963.

Yohannan, S., Yang, D., Faham, S., Boulting, G., Whitelegge, J., and Bowie, J.U. (2004b). Proline substitutions are not easily accommodated in a membrane protein. J. Mol. Biol. *341*, 1–6.

Zhang, X., Ren, W., DeCaen, P., Yan, C., Tao, X., Tang, L., Wang, J., Hasegawa, K., Kumasaka, T., He, J., et al. (2012). Crystal structure of an orthologue of the NaChBac voltage-gated sodium channel. Nature *486*, 130–134.

Neuron, Volume *84*

Supplemental Information

Transmembrane Helix Straightening and Buckling Underlies Activation of Mechanosensitive and Thermosensitive K_{2P} Channels

Marco Lolicato, Paul M. Riegelhaupt, Cristina Arrigoni, Kimberly A. Clark, and Daniel L. Minor, Jr.

Figure S1

Lolicato *et al.*

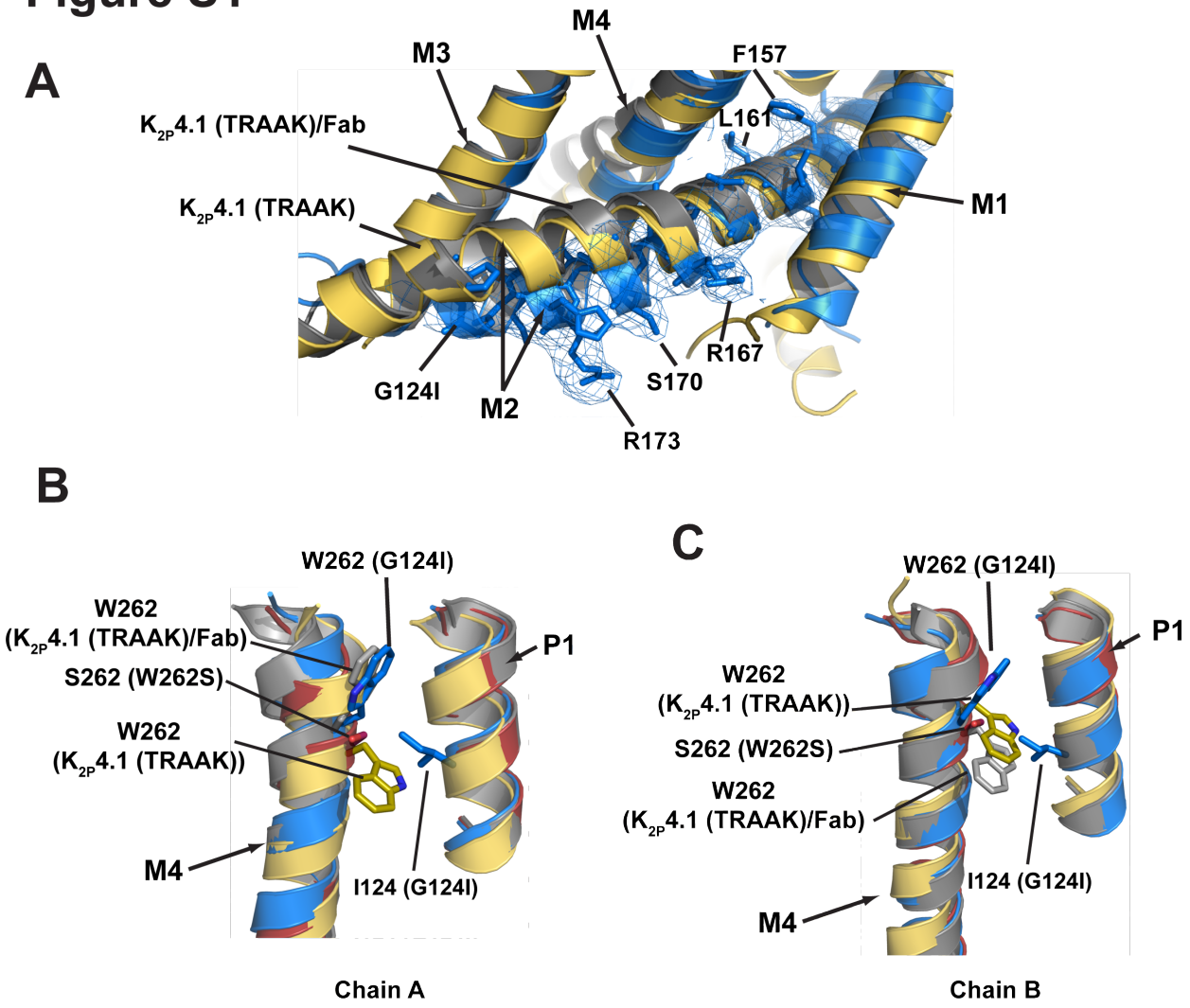

Figure S1, Related to Figure 1 Structures of K_{2P}4.1 activating mutants A, 2Fo-Fc electron density (marine mesh) for a portion of the G124I Chain A M2 helix (marine). Select residues are indicated. Cartoons depict G124I (marine), K_{2P}4.1 (TRAAK)/Fab (grey) (Brohawn et al., 2013) and K_{2P}4.1 (TRAAK) (Brohawn et al., 2012) (yellow). **B,** and **C,** Structural comparison of the M4 and P1 regions of G124I (marine), W262S (firebrick), K_{2P}4.1 (TRAAK)/Fab (grey) (Brohawn et al., 2013) and K_{2P}4.1 (TRAAK) (Brohawn et al., 2012) (yellow). Sidechains of residues 124 and 262 are depicted as sticks and are labeled.

Figure S2

Lolicato *et al.*

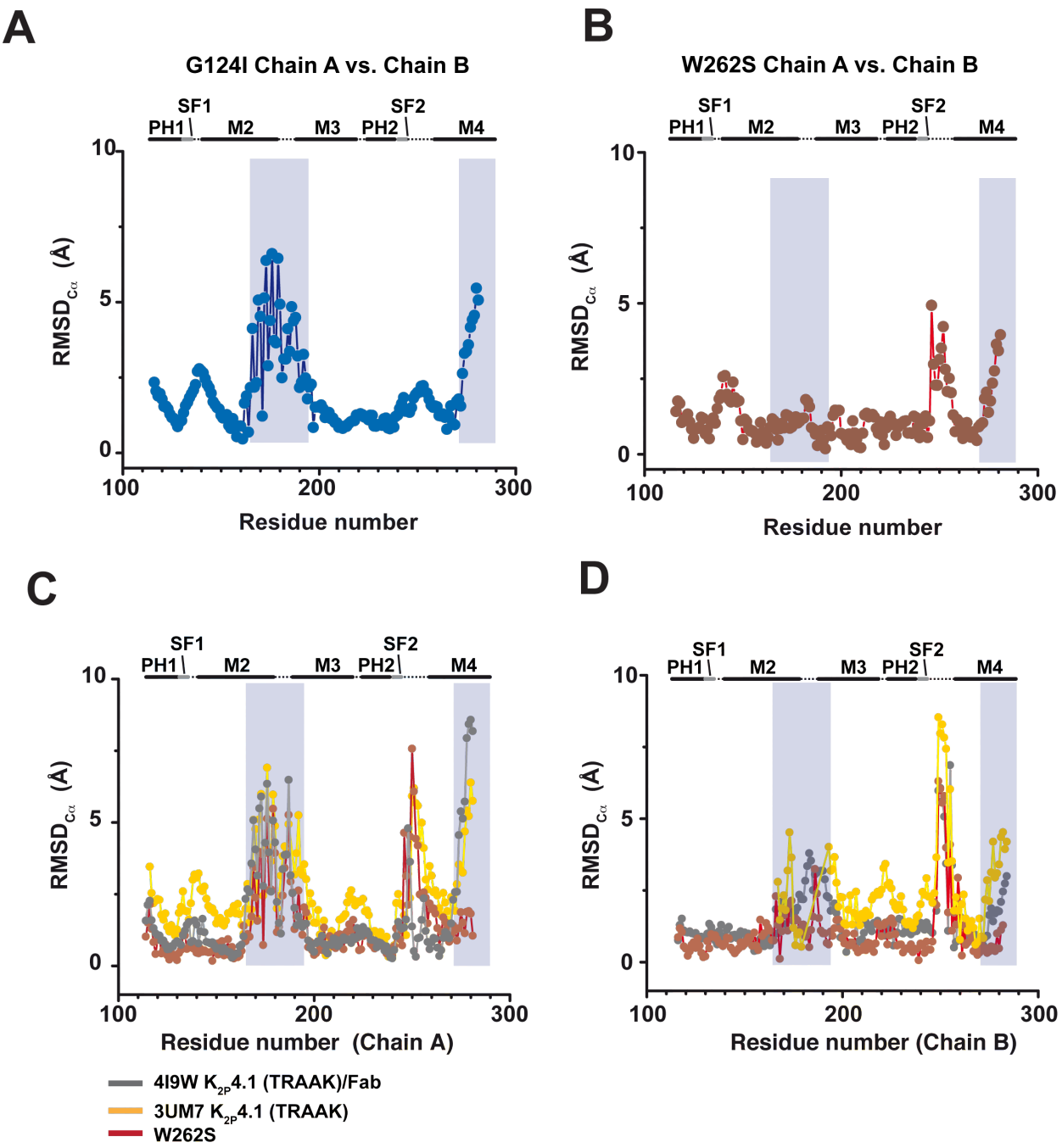

Figure S2, Related to Figure 1 K_{2P}4.1 (TRAAK) Residue by residue structure comparisons Cα RMSD plots comparing the indicated regions of **A**, G124I, Chains A and B, **B**, W262S, Chains A and B. **C** and **D** show comparisons of G124I Chain A with **C,** Chain A and **D,** Chain B from K_{2P}4.1 (TRAAK) (Brohawn et al., 2012) (yellow) K_{2P}4.1 (TRAAK) /Fab (grey) (Brohawn et al., 2013), and W262S (firebrick). Secondary structure elements are indicated as PH1 (pore helix 1), SF1 (selectivity filter 1), M2, M3, PH2 (pore helix 2), SF2 (selectivity filter 2) and M4. Shading indicates the buckled region of M2 and the portion of M4 C-terminal to the G238 bend.

Figure S3

Lolicato *et al.*

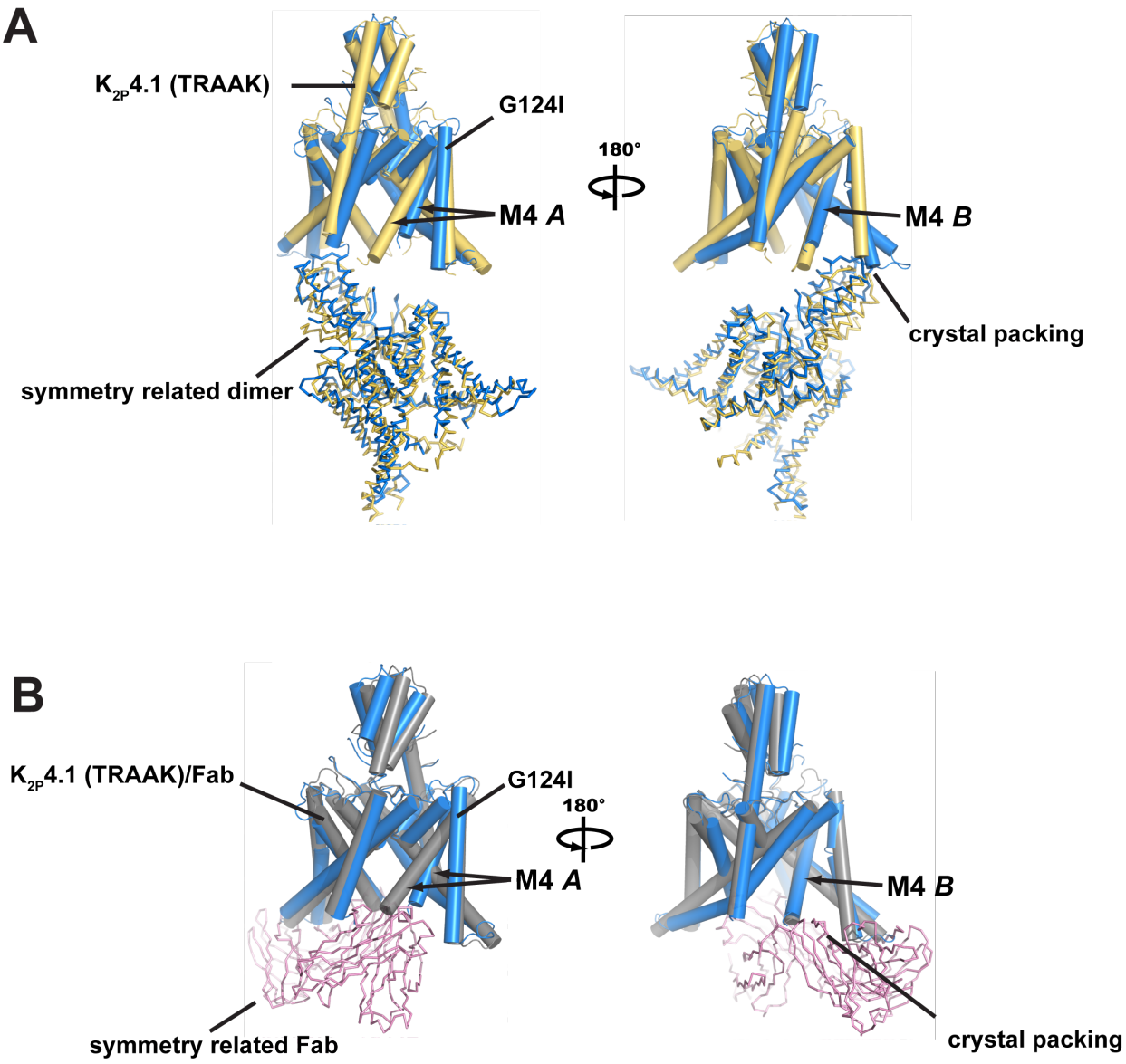

Figure S3, Related to Figure 1 Crystal packing contributes to K_{2P}4.1 (TRAAK) structural asymmetry Conformational differences between chain A and chain B with respect to crystal packing for **A,** K_{2P}4.1 (TRAAK) (Brohawn et al., 2012) (yellow) and **B,** K_{2P}4.1 (TRAAK)/Fab (grey) (Brohawn et al., 2013). In both cases the structure of G124I (marine) is shown for comparison. M4 helices of Chains A and B are indicated.

.

Figure S4

Lolicato *et al.*

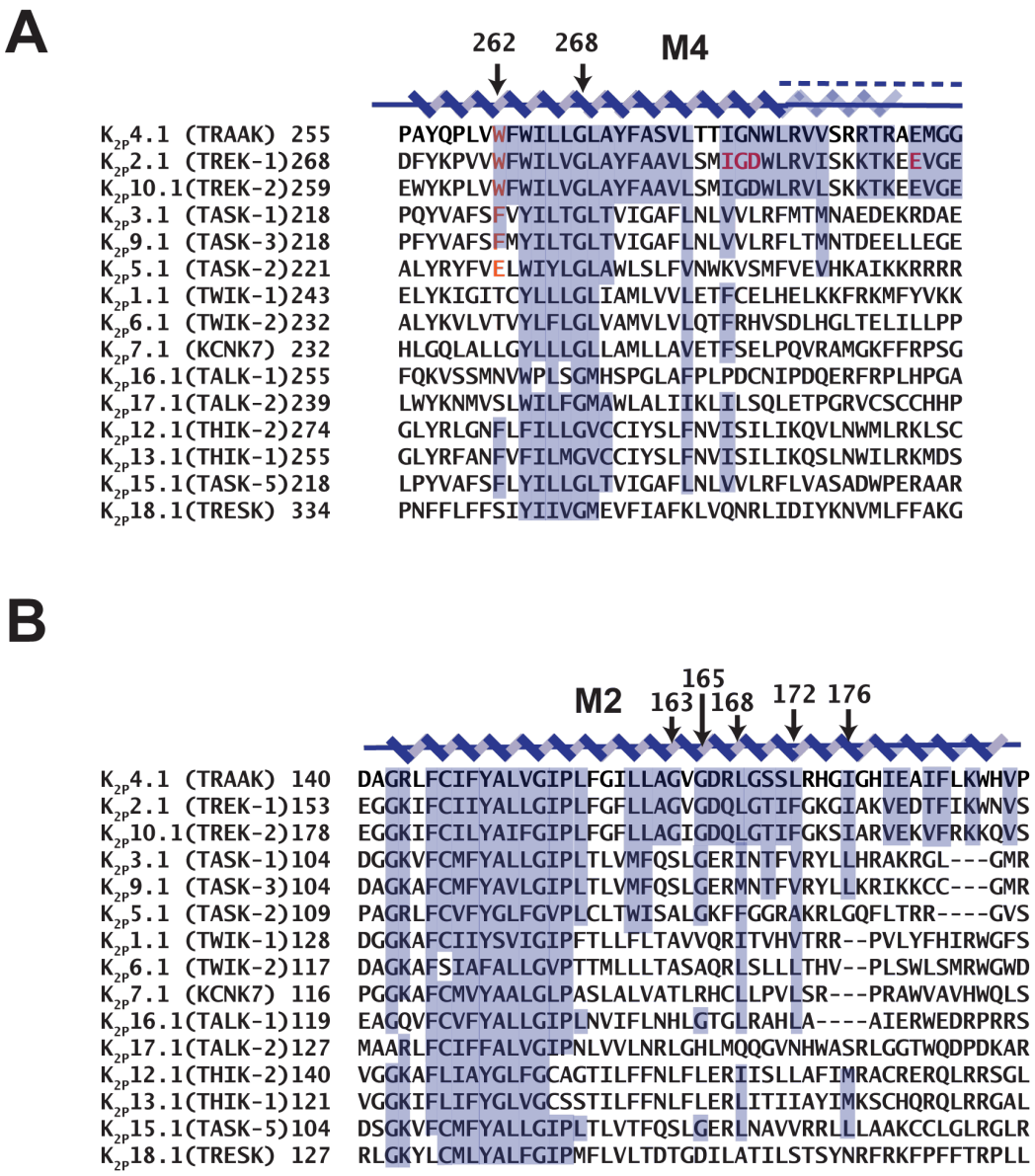

Figure S4, Related to Figure 3 Sequence comparisons of K_{2P} M4 and M2 helices Sequence alignment of **A,** M4 and **B**, M2 helices of the indicated K_{2P}s. Secondary structure is indicted. Dashed lines and pale cartoon indicate region of M4 where helical structure is absent in G124I and W262S. Position of W262S and the conserved glycine are indicated. Red residues indicate mutants that affect gating (Bagriantsev et al., 2012; Bagriantsev et al., 2011) and the site of an activating mutation in the C-terminal tail of K_{2P}2.1 (TREK-1) (Honore et al., 2002). For M2, conserved glycines of the 'GXG' motif and M2/M3 interface residues (168, 172, and 176) are marked. In both alignments, shading indicates conserved residues.

Figure S5

Lolicato *et al.*

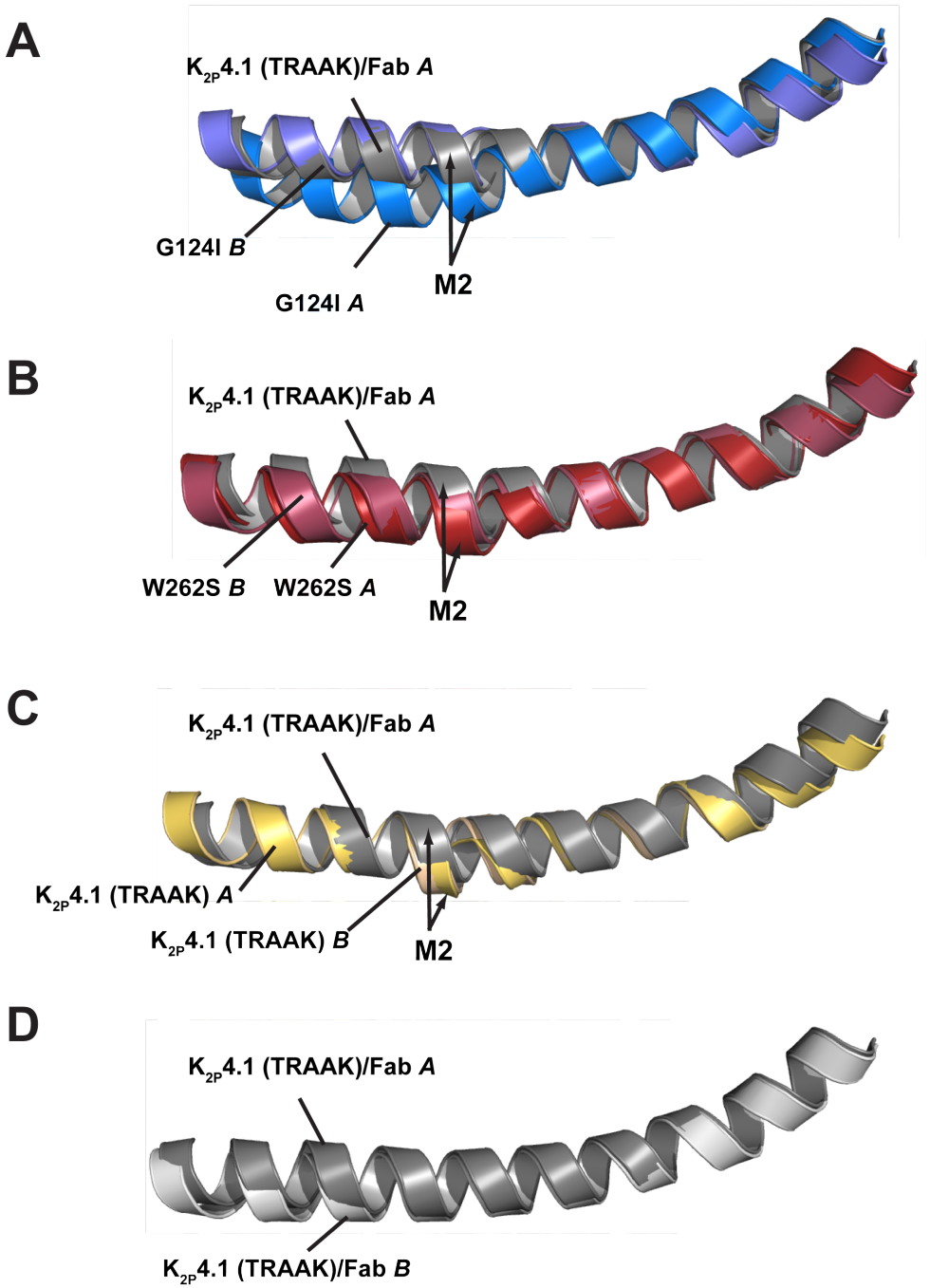

Figure S5, Related to Figure 4, Comparison of M2 conformations in Chain A and Chain B for A, G124I (marine and slate), **B,** W262S (firebrick and raspberry), **C,** K_{2P}4.1 (TRAAK) (yellow and sand) (Brohawn et al., 2012), and **D,** K_{2P}4.1 (TRAAK)/Fab complex (Brohawn et al., 2013). In A-B M2 of Chain A from the K_{2P}4.1 (TRAAK)/Fab complex (grey) (Brohawn et al., 2013) is shown for reference.

Figure S6

Lolicato *et al.*

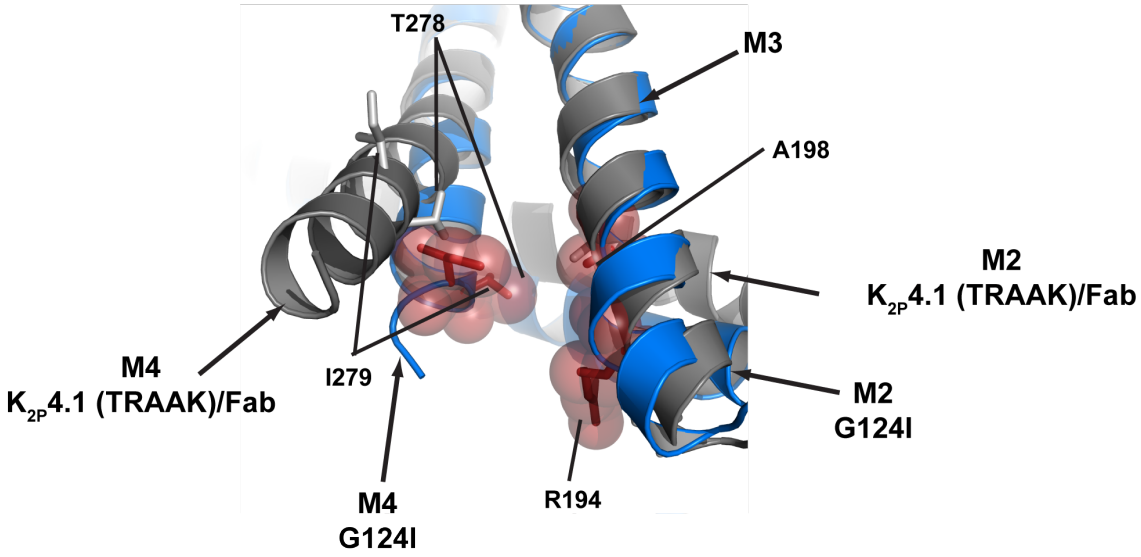

Figure S6, Related to Figure 8 Location of residues implicated in general anesthetic and covalent chemical activation responses Cytoplasmic view of a single subunit of K_{2P}4.1 (TRAAK) (grey) (Brohawn et al., 2013) and G124I (marine). Highlighted residues in K_{2P}4.1 (TRAAK) (white) and G124I (red) correspond to *Lymnea stagnalis* LyTASK (Andres-Enguix et al., 2007) and K_{2P}9.1 (TASK-3) (Andres-Enguix et al., 2007; Conway and Cotten, 2012) residues implicated in anesthetic responses and covalent activation at a Met→Cys mutant. K_{2P}4.1 (TRAAK) Ala198 corresponds to K_{2P}9.1 (TASK-3) Met159 and LyTASK L159. K_{2P}4.1 (TRAAK) Arg 194, Thr 278 and Ile 279 correspond to LyTASK S155, L241 and L242, respectively.

Supplementary Movie S1, Related to Figure 4 Conformational changes in a single K_{2P}4.1 (TRAAK) subunit Single subunit morph between the resting and activated conformations of K_{2P}4.1 (TRAAK) based on the K_{2P}4.1 (TRAAK)/Fab complex (grey) (Brohawn et al., 2013) and G124I (marine) structures, respectively. The channel is depicted in cartoon rendering to represent the backbone structure. M4 length corresponds to that seen in the G124I structure. Color changes to yellow and firebrick represent conformations similar to the K_{2P}4.1 (TRAAK) (yellow) (Brohawn et al., 2012) and W262S (firebrick) structures respectively.

Supplementary Movie S2, Related to Figure 5 Conformational changes in K_{2P}4.1 (TRAAK) Morph between the resting and activated conformations of K_{2P}4.1 (TRAAK) based on the K_{2P}4.1 (TRAAK)/Fab complex (grey) (Brohawn et al., 2013) and G124I (marine) structures, respectively. Structures contain two copies of chain A in which one has been superposed on the position of chain B and hence, are symmetric. The channel is depicted in cartoon rendering to represent the backbone structure. M4 length corresponds to that seen in the G124I structure. Color changes to yellow and firebrick represent conformations similar to the K_{2P}4.1 (TRAAK) (yellow) (Brohawn et al., 2012) and W262S (firebrick) structures respectively.

Supplementary Movie S3, Related to Figure 5 Surface rendered view of K_{2P}4.1 (TRAAK) conformational changes Morph between the resting and activated conformations of K_{2P}4.1 (TRAAK) based on the K_{2P}4.1 (TRAAK)/Fab complex (Brohawn et al., 2013) and G124I structures, respectively. Movie S3 is identical to Movie S1 but depicts the surfaces. This depiction highlights the opening of the lateral door to the inner bilayer. The channel is depicted in surface rendering. Color changes to yellow and firebrick represent conformations similar to the K_{2P}4.1 (TRAAK) (yellow) (Brohawn et al., 2012) and W262S (firebrick) structures respectively.

Supplementary Movie S4, Related to Figure 8 Cytoplasmic view of K_{2P}4.1 (TRAAK) conformational changes Cytoplasmic view of Movie S2.

Table S1, Related to Figure 1 K_{2P}4.1 (TRAAK) structural comparisons

	G124I vs. K_{2P}4.1 (TRAAK)/Fab	G124I vs. K_{2P}4.1 (TRAAK)	G124I vs. W262S	K_{2P}4.1 (TRAAK)/Fab vs. K_{2P}4.1
Cα RMSD				
Overall	2.13Å	4.80Å	1.54 Å	4.50Å
ΔM2, Δ∗M4	1.55Å	5.18 Å	0.95Å	5.05Å
ΔCAP	1.89 Å	2.20Å	1.59 Å	1.79Å
Channel Core (ΔCAP, ΔM2, ΔM4)	0.76 Å	1.29 Å	0.76 Å	1.00 Å

Definitions (RMSD calculated using the following channel elements of Chain A and Chain B)

Overall

M1 to M4 (residues 28-96 and 116-284), loop between CAP and PH1 was removed (residues 97-115))

ΔM2, ΔM4

M1 through CAP (residues 28-96), PH1 through common part of M2 (residues 116-160), and M3 through PH2 (residues 191-245)

ΔCAP

M1 (residues 28-56), PH1 through M4 (residues 110-284)

Channel core (ΔCAP ΔM2, ΔM4)

M1 (residues 28-56), PH1 through common part of M2 (residues 116-160), M3 through PH2 (residues 191-245) (the selectivity filter was included in the calculation).

For the non-domain-swapped K_{2P}4.1 (TRAAK), residues 28-96 of chain A were compared to equivalent residues on chain B.

Supplementary References

Andres-Enguix, I., Caley, A., Yustos, R., Schumacher, M.A., Spanu, P.D., Dickinson, R., Maze, M., and Franks, N.P. (2007). Determinants of the anesthetic sensitivity of two-pore domain acid-sensitive potassium channels: molecular cloning of an anesthetic-activated potassium channel from Lymnaea stagnalis. J Biol Chem *282*, 20977-20990.

Bagriantsev, S.N., Clark, K.A., and Minor, D.L., Jr. (2012). Metabolic and thermal stimuli control K(2P)2.1 (TREK-1) through modular sensory and gating domains. EMBO J *31*, 3297-3308.

Bagriantsev, S.N., Peyronnet, R., Clark, K.A., Honore, E., and Minor, D.L., Jr. (2011). Multiple modalities converge on a common gate to control K2P channel function. EMBO J *30*, 3594-3606.

Brohawn, S.G., Campbell, E.B., and MacKinnon, R. (2013). Domain-swapped chain connectivity and gated membrane access in a Fab-mediated crystal of the human TRAAK K+ channel. Proc Natl Acad Sci U S A *110*, 2129-2134.

Brohawn, S.G., del Marmol, J., and MacKinnon, R. (2012). Crystal structure of the human K2P TRAAK, a lipid- and mechano-sensitive K+ ion channel. Science *335*, 436-441.

Conway, K.E., and Cotten, J.F. (2012). Covalent modification of a volatile anesthetic regulatory site activates TASK-3 (KCNK9) tandem-pore potassium channels. Molecular pharmacology *81*, 393-400.

Honore, E., Maingret, F., Lazdunski, M., and Patel, A.J. (2002). An intracellular proton sensor commands lipid- and mechano-gating of the K(+) channel TREK-1. EMBO J *21*, 2968-2976.